1991

Human factors engineering in sonar visual displays.

Galvin, Lawrence Francis

Springfield, Virginia: Available from National Technical Information Service

http://hdl.handle.net/10945/28265

HUMAN FACTORS ENGINEERING IN SONAR VISUAL DISPLAYS

by

LAWRENCE FRANCIS GALVIN

B. S. Mathematics, United States Naval Academy
(1978)

Submitted in Partial Fulfillment of the
Requirements for the Degree of

MASTER OF SCIENCE in OCEANOGRAPHIC ENGINEERING

at the

MASSACHUSETTS INSTITUTE OF TECHNOLOGY

and the

WOODS HOLE OCEANOGRAPHIC INSTITUTION

August 1991

HUMAN FACTORS ENGINEERING IN SONAR VISUAL DISPLAYS

by

LAWRENCE FRANCIS GALVIN

Submitted to the Massachusetts Institute of Technology/
Woods Hole Oceanographic Institution
Joint Program in Oceanographic Engineering
on August 30, 1991, in partial fulfillment of the
requirements for the degree of

MASTER OF SCIENCE IN OCEANOGRAPHIC ENGINEERING

Abstract

Undersea technology is on the verge of equipping remotely operated vehicle (ROV) pilots with a three-dimensional (3-D), real-time display incorporating data from a wide variety of sensors including sonar (sound navigation and ranging), cameras, and lasers. Effective collection, computation, and presentation of this data to the pilot in a single display presents hardware, software and human factors problems. This thesis focuses on human factors issues associated with the display of information which could enhance the pilot's efficiency of performance. Background information on human factors engineering, 3-D computer graphics displays, and application of the 3-D perspective display precede the details of the experiment.

Five specific display enhancements tested include altering the displayed field of view, providing a screen grid, displaying the current range to the target of interest, using a vertical color scheme, and controlling the display update rate. Seven tests measure the effects of these display enhancements on the simulated piloting of an ROV. The effects of the ROV simulation and operator learning curves are removed to compare performance changes due to the various enhancements directly. Operator comments during and after testing as well as test monitor/author observations provide insight into the experiment. Test result implications for system design trade-offs are discussed in detail. Recommendations for future research and the proposed construction of a fully equipped ROV simulator complete the work.

Thesis Supervisors:

Dr. W. Kenneth Stewart
Assistant Scientist, Deep Submergence Laboratory
Woods Hole Oceanographic Institution

Dr. Thomas B. Sheridan
Professor of Engineering and Applied Psychology
Massachusetts Institute of Technology

Acknowledgements

Initially, I wish to thank the United States Navy for this unsurpassed opportunity to improve myself professionally.

A number of individuals contributed directly to the completion of this work. Key computer programming assistance was provided by Charlie Chafouleas and Dan Potter. Tagore Somers and Martin Bowen of the Marquest Group, Inc., lent equipment. Will Sellers and Skip Gleason injected their ROV pilot experience. Rob Keefe, Hanu Singh, Gary Edwards, and Tom Riggle each spent many hours flying the simulator. Special thanks is due to CDR John Halsema, USN, Dr. Dana Yoerger, and Dr. Gene Terray.

Sincere gratitude is due to Raymond A. Sullivan, M.D. and Thomas F. Gregg, M.D., for services rendered.

I have been fortunate to have two extremely knowledgeable, capable, and respected thesis advisors in Dr. Ken Stewart (WHOI) and Dr. Tom Sheridan (MIT). Perhaps the greatest professional contribution to my work was provided by Dr. Stewart, who for the entire two years of my stay has understood even better than I the rigors of raising a family while attending graduate school.

Without doubt, the greatest personal contribution to my work came from my wife Atti. In our short tour here she has given birth to two healthy baby boys (Danny - June 15, 1989 and Timmy - March 27, 1991) while continuing to run the house and our oldest son Andy (September 14, 1987). She is living proof of the saying: "Navy Wife - It's the toughest job in the Navy."

Finally, I must offer my appreciation to people of the Woods Hole Oceanographic Institution. Top to bottom it is the singularly finest working environment it has been my great pleasure to experience.

Dedication

To my most special wife Atti

and

our wonderful sons Andy, Danny, and Timmy.

Table of Contents

List of Figures

List of Tables

Chapter 1

Introduction

1.1 Background

Sonar (Sound Navigation and Ranging) is a technique for underwater range finding that has existed for more than fifty years. The author's thirteen years of experience with military and commercial sonars indicate that the techniques employed to present sonar information to the user significantly lag the technology used in areas such as hardware design, beam forming, and data processing, and unnecessarily limit the bandwidth of information transfer. The wide variety of display designs and information formats proves confusing to all but the most adept and experienced users. Additionally, the typical restriction of the presentation to two coding dimensions, coincident with the physical dimensions of the cathode ray tube (CRT), severely restricts the ability to effectively convey large amounts of data.

The Woods Hole Oceanographic Institution's (WHOI) Deep Submergence Laboratory (DSL) operates several seagoing craft including remotely operated vehicles (ROVs), whose pilot "flies" the deep-diving ROV from an operations center located on a mother ship on the surface above. Within video camera range the pilot's display resembles the view a driver sees out the front windshield of an automobile, with some loss of depth perception. This video display format is "natural" for the pilot and provides a large information transfer bandwidth. Suspended sediment near the bottom frequently limits the already restricted visual range of camera equipment to a couple of meters. Beyond visual range the pilot

must rely on the customary two-dimensional (2-D) active (transmit and receive) sonar presentations.

Technological advances currently provide the capability to combine undersea data from a number of sensors including active sonars, video tape and electronic still cameras, manipulators, and laser range finders. These data can be assimilated and processed in real time to provide large quantities of high quality information. The data generated can be used to provide the ROV pilot with a real-time, three-dimensional (3-D), perspective display similar to that of the video camera when beyond visual range. This more natural view would ease the pilots workload and improve the efficiency of work conducted beyond visual camera range. Such a perspective-view display is expected to be dominated in the foreground by high-resolution video data, gradually transitioning to dominance by other sensors as the limits of video range are encountered. The envisioned 3-D display must be carefully designed to best improve the ROV pilot's efficiency.

1.2 Research Objectives

A variety of display enhancements have been used in military and commercial sonars. This thesis looks at the individual effects of six specific display enhancements: widening the field of view (FOV) to provide more information to the pilot, 2-D and 3-D gridding for improved angular and depth perception, vertical color schemes for better altitude versus depth perception, direct range readout to shorten the search and location cycle, and shortening the display update rate. Seven experiments to isolate and quantify the individual effects of these enhancements are described in detail. The analysis allows direct comparison of the effectiveness of the six enhancements.

1.3 Terminology

Terminology is critical to comprehension. Several important definitions include:

- altitude - the distance above the floor of the ocean.
- data - "raw" numbers from which information can be extracted.
- data point - one of a set of 25 x, y, and z coordinates chosen for a target course.
- depth - the perceived distance into a video or computer display. This is a spatial perception of range.
- display - the computer screen dedicated to graphics information.
- driving - the act of operating the simulated ROV for testing.
- heading - the compass direction in which the vehicle is pointed.
- monitor - the computer screen dedicated to printed information, including update indication,"target hit" and "mission complete" indication, target range indication (test 6), and vehicle world-coordinate position, heading, and velocities. This term is also used to describe the actions of the author as the testing supervisor.
- operator - a test subject who drove the simulated ROV.
- pilot - a qualified flyer of operational ROVs.
- piloting - the act of flying a operational ROV.
- target - the numbered, cubic wireframe, data point visualizing tool.
- target course - one of 19 (lettered A-R, X) specific sequences of data points and associated targets.
- update - the complete refreshing of a computer screen.
- vertical - the direction opposite to that in which gravity acts. A vertical color scheme encodes altitude information using a color scale or look-up table.

1.4 Overview

Chapter 2 provides background information on human factors engineering and its relationship to the thesis work.

Chapter 3 contains information on three-dimensional computer graphics displays in general, and the display and equipment used in the thesis experiments.

Chapter 4 discusses current and projected applications of three-dimensional perspective displays in underwater visualization.

Chapter 5 describes in detail the conduct of seven tests including restricting the field of view, grids to provide depth and angular cues, color schemes to provide altitude cues versus depth of field, direct range information, and slowing of the graphic display update rate.

Chapter 6 presents the results of the seven tests including operator comments and author/test monitor observations.

Chapter 7 summarizes the results of the experiments, discusses conclusions, and offers recommendations for future work.

Chapter 2

Human Factors Engineering

2.1 Objectives and Doctrines

Human factors engineering is the study of people and how equipment designs affect them. The two major objectives of human factors engineering are to improve efficiency and effectiveness and to promote key elements such as safety, satisfaction, and stress reduction. Six doctrines that form a set of human factors commandments are [S-1]:

- Design with the user in mind.
- Recognize differences in capabilities and limitations of people and their design implications.
- Design influences human behavior.
- Design process includes empirical data and evaluation.
- Reliance on scientific methods and objective data.
- Commitment to system orientation.

2.2 Methodology Issues

Experimental research methods test the effects of variables on behavior. Of prime interest in this work is the behavior "efficiency of operator performance". The method

selected needed to accurately measure this efficiency. Eight important issues associated with the choice of methodology are [M-1]:

- Effectiveness.
- Ease of use.
- Cost.
- Flexibility.
- Range.
- Validity.
- Reliability.
- Objectivity.

No approach was best for all the issues above. Among them effectiveness, validity, reliability, and objectivity were deemed most critical for this thesis. Validity, in particular, was enhanced by input from experienced ROV pilots and operational support group personnel. These inputs served to more realistically match the simulation to operating conditions.

2.3 Research Criteria

Research criteria can be divided, with inevitable overlap, into the areas of system-descriptive criteria, task-performance criteria, and human criteria [M-1]. The criteria chosen for analysis in this work was task performance, specifically performance time. Human criteria cannot be ignored, however, and provide insight in the form of subjective comments by the operators, both during and after each test, and observations by the test monitor/author.

2.4 Visual-Coding

Color is a prime visual-coding technique. It has been frequently used in 3-D underwater visualization to provide depth/relief cueing in the form of a continuous color scale versus depth. In this work two discrete color sets were chosen for testing. Both the 6- and 21-color sets were derived from the red, green, and blue (RGB) color model. Figure 2.1 shows the RGB cube [F-1]. The 6-color set was selected by following a path from corner to corner in the following order: red, yellow, green, cyan, blue, and magenta. The 21-color set followed the same path, selecting colors at each 0.25-unit path-length increment.

The designation of specific color names was complicated by the existence of a variety of descriptive systems. Among the more notable were RGB, HSB, Munsell, ISCC-NBS, YIQ, CIE, and UCL [B-1, F-1, K-1]. Target color names were derived starting with the basic six colors of the RGB color set (identical to the six basic hues of the HSB color set): red, yellow, green, cyan, blue, and magenta [F-1]. The further subdivisions were named in accordance with the spirit of the Color Naming System (CNS), which was developed to simplify color descriptions [B-1]. The 21 color names derived were used for the 1-, 6-, and 21-color sets. Table 2.1 lists the colors by name and includes RGB and HSB descriptions. Conversions between most color sets were available and easily done with a computer program [F-1].

2.5 Control and Tracking Performance

Controls transmit discrete or continuous signals to a system to produce a desired response. Important factors in control design include ease of identification, size, control-response ratio, resistance, lag, deadspace, backlash, location, and compatibility [S-1].

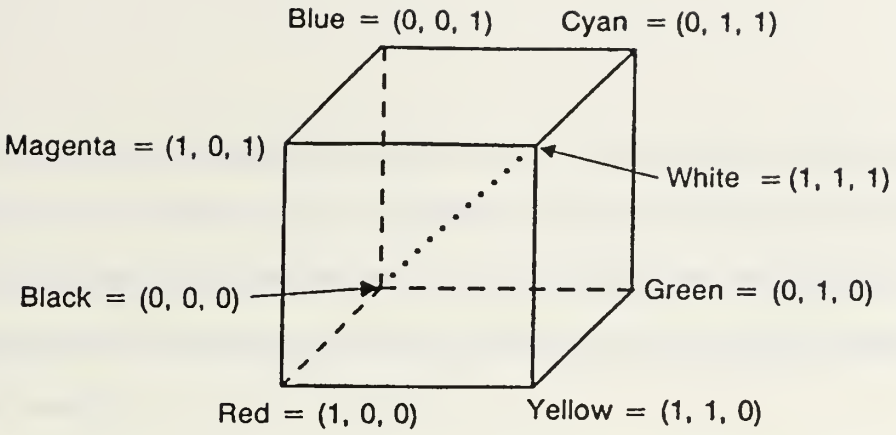

Figure 2.1 The RGB (red, green, and blue) cube [F-1]

Table 2.1 Color set RGB to HSB conversion

Color	Red	Green	Blue	Hue	Saturation	Brightness
Red	1	0	0	0	1	1
Reddish Orange	1	0.25	0	15	1	1
Orange	1	0.50	0	30	1	1
Yellowish Orange	1	0.75	0	45	1	1
Yellow	1	1	0	60	1	1
Yellowish Yellow-Green	0.75	1	0	75	1	1
Yellow-Green	0.50	1	0	90	1	1
Greenish Yellow-Green	0.25	1	0	105	1	1
Green	0	1	0	120	1	1
Greenish Aquamarine	0	1	0.25	135	1	1
Aquamarine	0	1	0.50	150	1	1
Cyanish Aquamarine	0	1	0.75	165	1	1
Cyan	0	1	1	180	1	1
Cyanish Turquoise	0	0.75	1	195	1	1
Turquoise	0	0.50	1	210	1	1
Blueish Turquoise	0	0.25	1	225	1	1
Blue	0	0	1	240	1	1
Blueish Purple	0.25	0	1	255	1	1
Purple	0.50	0	1	270	1	1
Magentaish Purple	0.75	0	1	285	1	1
Magenta	1	0	1	300	1	1

Deadspace refers to a null established about the control's normal position in which control device motion results in no signal output. Backlash is deadspace at all control positions. The control mechanism may have no resistance (free-positioning or *pure-displacement* control), no displacement (stiff stick or *pure-force* control), or lie in the middle (which we term a *mixture* control).

The control order of a system refers to the relationship between the control mechanism and the system output. Orders of control include [S-1]:

- position (zero-order) control - where the signal controls the output directly.
- velocity (first-order) control - where the signal controls the rate of change of position.
- acceleration (second-order) control - where the signal controls the rate of change of velocity.
- higher-order control - where the signal controls the rate of change of acceleration or other higher order term.

The system in these tests used second-order control of thrust, equivalent to acceleration, in each of the four degrees of freedom (see Section 5.3).

The problem presented to the operator was a compensatory tracking problem with time lag [S-1]. The time lag was composed of three parts:

- response lag - the time required for the operator to choose and execute a response.
- control system lag - the time required for the system to respond to commands including vehicle motion simulation.
- display system lag - the time required for graphics calculations and display update.

In each case the time lag increased tracking error.

2.6 Test and Evaluation

Independent variables (IVs) are those parameters controlled by the experimenter. Dependent variables (DVs) are measured parameters affected by the IVs. They are the same as the research criteria discussed in Section 2.3.

Evaluation of test results must consider test subjects, criteria, and experimental procedures [S-1]. Subjects should be representative of projected users. Dependent variables (criteria) must be related to system operational use. Experimental procedures and controls should give repeatable results.

Chapter 3

Three-Dimensional Computer Graphics Displays

3.1 True 3-D Displays

Technology stands at the threshold of true three-dimensional displays. Available implementations display depth instead of simply providing depth cueing. Two such systems are SpaceGraph™ by Bolt, Beranek, and Newman (BBN) Laboratories Incorporated of Cambridge, Massachusetts and OmniView™ by Texas Instruments (TI) of Dallas, Texas.

The SpaceGraph™ system is based on reflecting a point plotted (not raster scanned) image in a vibrating mirror. The technique is termed the *varifocal mirror*. As the reflecting surface vibrates it repeatedly changes shape from concave to convex, causing a large change in focal length. When the image update rate is synchronized with the mirror vibration, a true 3-D image is created in space. For many data-set analyses the superior pattern-recognition capability of the human brain is enhanced by this type of display. This system is limited in viewing angle, display update rate, and to simple monochrome images. [F-1, T-1, S-2]

The OmniView™ system is based on laser scanning of a paraboloidal, rapidly rotating surface. During rotation, the scanning laser beam's reflections form the 3-D image. Advantages include 360° horizontal viewing and total wrap-around parallax. This system has no hidden surface removal and cannot display solid surfaces. [E-1]

Holography is another promising technology for true 3-D viewing. This work is based on the splitting of a laser beam into two parts, illumination of objects by one of the split beams, and their subsequent recombination using the second beam as a reference. Limitations typically include small size and restricted viewing angle, lack of parallax, and high cost. [E-1, F-1]

Head-mounted displays have offered tremendous potential since their birth in the late 1960s [S-3, S-4]. The helmeted user enjoys freedom of movement in a virtual 3-D world projected in real time for separate viewing by the each eye. Technical problems have severely restricted the development of this technology since its inception [F-1].

An inherent limitation of true three-dimensional viewing is the tremendous quantity of data and associated data processing, particularly critical for real-time display. Expenses for computation rise dramatically as realistic, complex 3-D imagery is approached and parallel-processing supercomputers become a necessity. Significant effort and funding are being funnelled into this cutting-edge technology, but it is not likely to be available to the field scientist before the late 1990s.

3.2 Simulated 3-D Displays

In the absence of true 3-D displays several methods are employed to simulate three-dimensional viewing using two-dimensional CRTs. These methods are designed to counter the information loss inherent in projecting 3-D information on a 2-D surface such as a computer screen. Techniques used include those for line drawings and shaded images, as well as dynamics, stereopsis, and head-motion parallax.

Line drawing techniques include the use of various projections, depth cueing with intensity, depth clipping, and hidden-line removal [F-1]. Among the projections, the perspective offers two significant depth cues: decreasing size of objects with depth and the

convergence of parallel lines to their vanishing points. Depth cueing with intensity draws the more distant objects at a lower intensity. The result is a strong depth cue similar to that observed when viewing a scene in a light fog. Depth clipping limits the view by preventing the drawing of lines not within the designated limits of the front or back clipping planes. This effect is used to limit the depth of field. Hidden line removal calculates the lines that should not be visible based on the view and does not draw them.

Shaded-image techniques include hidden-surface removal, control of illumination and shading, various shading interpolation methods, and the use of texture, shadows, transparency, and reflection.

Dynamics refers to the added information available when a sequence of views is shown instead of a static view. The primary depth cue is provided by the kinetic depth effect, the lower velocity of nearby objects versus those in the background.

Stereopsis is a depth cue taking advantage of the binocular disparity between human eyes [F-1]. The ability of the human brain to fuse two slightly differing views of a scene and extract depth information is a powerful depth cue.

Head-motion parallax uses the changing view as occurs in real life when the head is moved side to side.

3.3 The Marquest System

Several important components of the test equipment hardware and software were provided by the Marquest Group, Inc. of Bourne, Massachusetts. They include the joystick module and associated software, an Nth Engine/550™ Display Controller, and HOOPS™ graphics routines and HYDRA™ rendering software for the Nth Engine/550™. They are components of a commercial ROV control system.

The joystick module is a standardized control device for ROVs constructed by the Marquest Group, Inc. using off-the-shelf components. Included are a trackball, bias and

gain potentiometers, nine push-button switches, and a 3-axis joystick. Only the joystick was used in the testing. Measurement Systems, Inc. of Norwalk, Connecticut, built the industry standard, heavy duty, 3-axis (x, y, θ) joystick with mixture control and deadspace on each of the three axes. A thumb switch provided the fourth axis of freedom (z) with pure force control. Another joystick available from Measurement Systems, Inc., but not used here, incorporated the fourth axis of freedom through lifting/depressing the joystick vertically with mixture control. Joystick use is discussed in Chapters 6 and 7.

The Nth Engine/550™ Display Controller is a 3-D graphics processor/controller built by Nth Graphics of Austin, Texas. The controller has 1280 x 1024 resolution and operates at 20 MIPS and 3 MFLOPS. The board set includes an NthTV™ converter module, which provides a standard commercial television format (NTSC) tap for direct, real-time recording of the video display on a video cassette recorder (VCR).

HOOPS™ from Ithaca Software of Ithaca, New York, formed an interactive three-dimensional graphics library. This software controlled the Nth Engine/550™.

HYDRA™ rendering software, another product of Nth Graphics, was used to convert targets and grids drawn in AutoCAD® Release 10 to the required format for the HOOPS graphics routines. A helpful feature is the ability to quickly conduct a visual check of targets and grids.

3.4 The Display and the Monitor

Planar geometric projections fall into two categories: perspective and parallel. Characteristics which distinguish a perspective projection from a parallel projection are convergence of parallel lines, size diminution, and nonuniform foreshortening [C-1]. The primary advantage of a perspective projection is the natural appearance of objects seen by the eye. It was also the standard video camera projection. For these reasons a three-point

perspective projection was chosen for the display [C-1]. The graphics were shown on a Sony model GDM-1950 19-inch color monitor with 1280 x 1024 pixel resolution.

Of the previously discussed techniques to provide three dimensionality, depth cueing in particular, many were not available in the experimental system for three reasons: the tests used a perspective projection, the targets were drawn in wireframe mode, and limitations of the Nth Graphics boards and software running the display. Depth cueing was provided by target relative size (because they were all identical in dimension), the convergence of parallel lines (emphasized by the cubic wireframe targets), and the kinetic depth effect.

An NEC VGA color monitor (with blue background) provided the following:

- display update indicated by the word "Busy.." appearing in white letters in a red box.
- most recent target hit indicated by the words "OBJECT #(target number) HIT" appearing in white letters in a red box.
- test completion indicated by the words "MISSION COMPLETE" appearing in white letters in a red box.
- range in meters from the vehicle (modelled as a point) to the center of the next target indicated by the symbol "R = (range)" appearing in white letters in a red box. This information was provided to the operator only during test 6.
- world system coordinates (x, y, and z) and heading of the vehicle in white numerals. Titles (xpos, ypos, zpos, and hdg) were shown beside the coordinates/heading in white letters.
- vehicle system velocities ($\dot{x}$, $\dot{y}$, $\dot{z}$, and θ rate) in white numerals. The titles (xvel, yvel, zvel, and rvel) shown in black letters above the velocities were individually accented with small red boxes if their magnitudes exceeded 0.05 m/s or 0.05 rad/s.

Figure 3.1 shows the monitor screen with range information during test 6 .

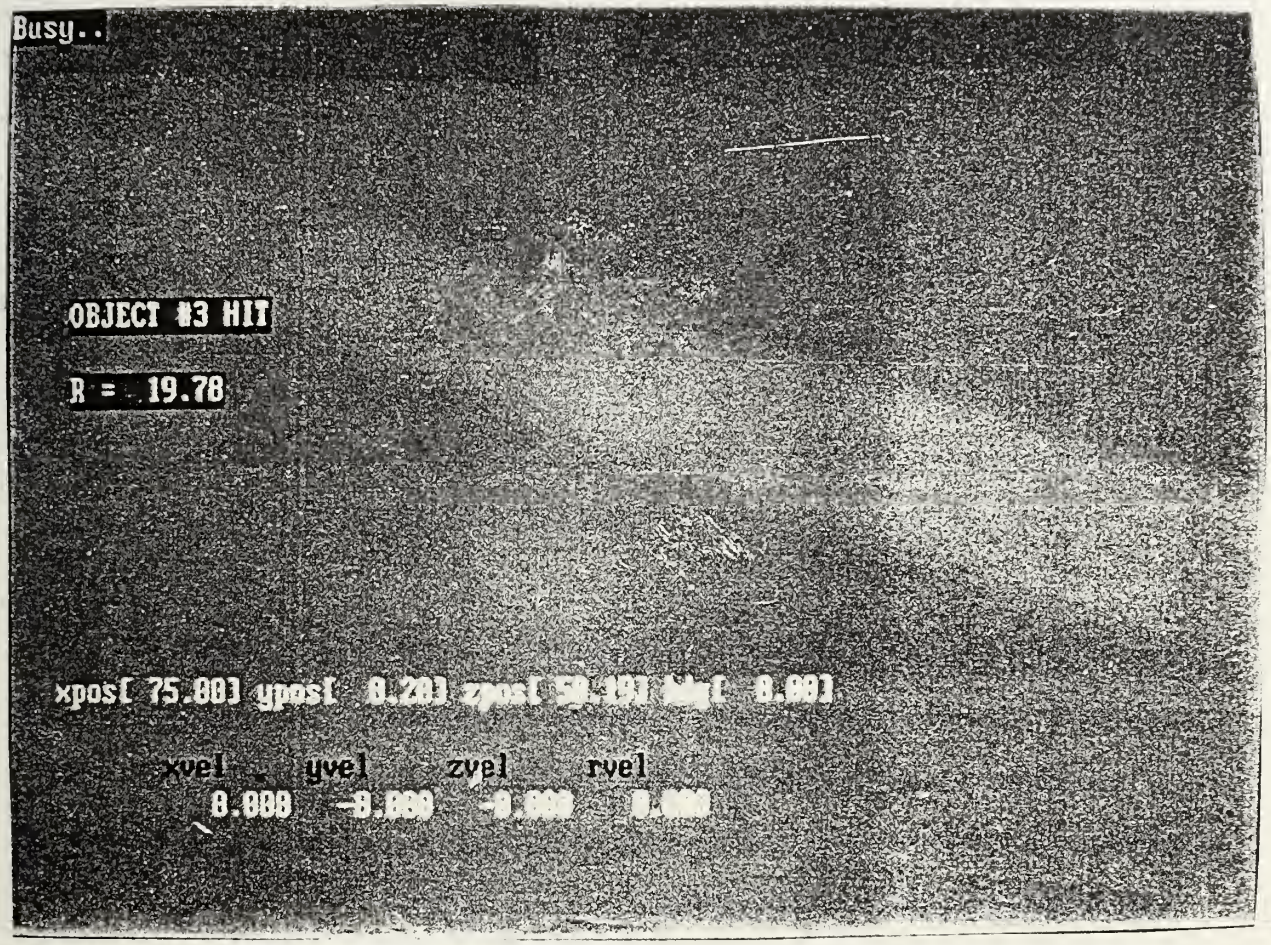

Figure 3.1 Monitor screen during test 6

Chapter 4

Application of the 3-D Perspective Display

4.1 Ocean Environmental Sensing

Early sonar development was driven by military needs. Crude processing and display techniques limited these systems to deterministic methods with severely restricted dynamic range. Inherent in these limitations were a disregard for inaccuracies such as angular and range resolution, variations in the speed of sound and the sound ray paths, and navigation errors in position, attitude, depth and motion. The current state of technology overcomes many of these restrictions. Modern computers and software graphics packages allow real-time processing and display of more advanced models of the ocean environment. New commercial sonars provide more accurate information from a variety of sampling techniques including swath mapping, sidescan, and upward-looking sonars, in addition to the more traditional forward-looking and bathymetric sounding versions. Innovative electronic instruments provide high-accuracy navigational data. Recent trends have resulted in additional technologies being adapted for underwater work. Video and electronic still cameras, and scanning lasers are among these supplementary sensors.

4.2 Multisensor Modeling

To effectively combine the various sensor modalities into a single model of the ocean environment, we must first accept the premise that no measurement is exact. Any information gathered will have an associated probability distribution, which is itself not known deterministically. The ocean model can be built incorporating these uncertainties as a stochastic model. This approach is especially effective when combining information from different sources with their differing ranges, resolutions, and data types. At any time, a deterministic model can be extracted from the current probabilistic one. Using this method, a more accurate deterministic model is obtained which accounts for the many and varied errors inherent in measurements.

Initially, the ocean volume of interest is divided into a 3-D grid of cubic volume elements, or voxels. The size of the voxels is dependent upon the desired model resolution as well as system hardware and software limitations for real-time processing. Each voxel is assigned a "feature" vector incorporating information such as the time, the position of the voxel in the coordinate space, the measured characteristics of interest (features), and a probability or confidence value for each feature. As new information is collected, older data is not discarded. Feature vectors are incremented using a data merging technique called *stochastic backprojection* [S-5, S-6]. This data merging technique is an adaptation of the backprojection and summation method used to reconstruct images. The method is enhanced to include probabilistic uncertainty and allow stepwise solutions for real-time processing. Use of these techniques allows combination of the redundant feature data from all available sources, improving the model resolution and certainty.

4.3 The Deep Submergence Laboratory System

The Deep Submergence Laboratory of the Woods Hole Oceanographic Institute employs a variety of sensors and platforms. A typical cruise involves flying equipment to a proximate port and loading out a chartered mother vessel. At the research site, a large area survey is conducted with a towed 120-kHz split-beam sonar system. This survey provides medium resolution imaging with a swath width of 200-300 meters at a tow speed of 6-10 knots, and allows items of interest to be identified for subsequent revisiting with higher resolution equipment. Items of interest are reinspected using the tethered Jason ROV system. Jason is typically equipped with a SHARPS short-baseline navigation system and a sensor package including a 200-kHz sidescan sonar, a 300-kHz forward-scanning sonar, a video camera, an electronic still camera, and a laser rangefinder. Figure 4.1 shows the range and resolution overlaps between sensors in the current suite.

The Jason pilot has several sources of information available. If within visual range, the video camera and vehicle lighting system provide a natural, perspective view with extremely high bandwidth. This visual range is often restricted to a meter or less due to suspended sediment in the water, and is usually less than about 10 meters. Beyond visual range the forward-scanning sonar, the 200-kHz sidescan sonar, the laser rangefinder, and the SHARPS navigation system provide data to several displays with differing formats. The pilot navigates using a specially designed 2-D auxiliary display with limited bandwidth until within visual range [S-7].

This current method taxes the pilot, whose task is complicated by [S-7]:

- low visibility, reducing video camera range and safe working speeds.
- the narrow field of view of the video camera (approximately 40°).
- the monocular vision of the video camera.
- optical distortion of the video camera.
- the difficulty of interpreting sonar presentation screens.

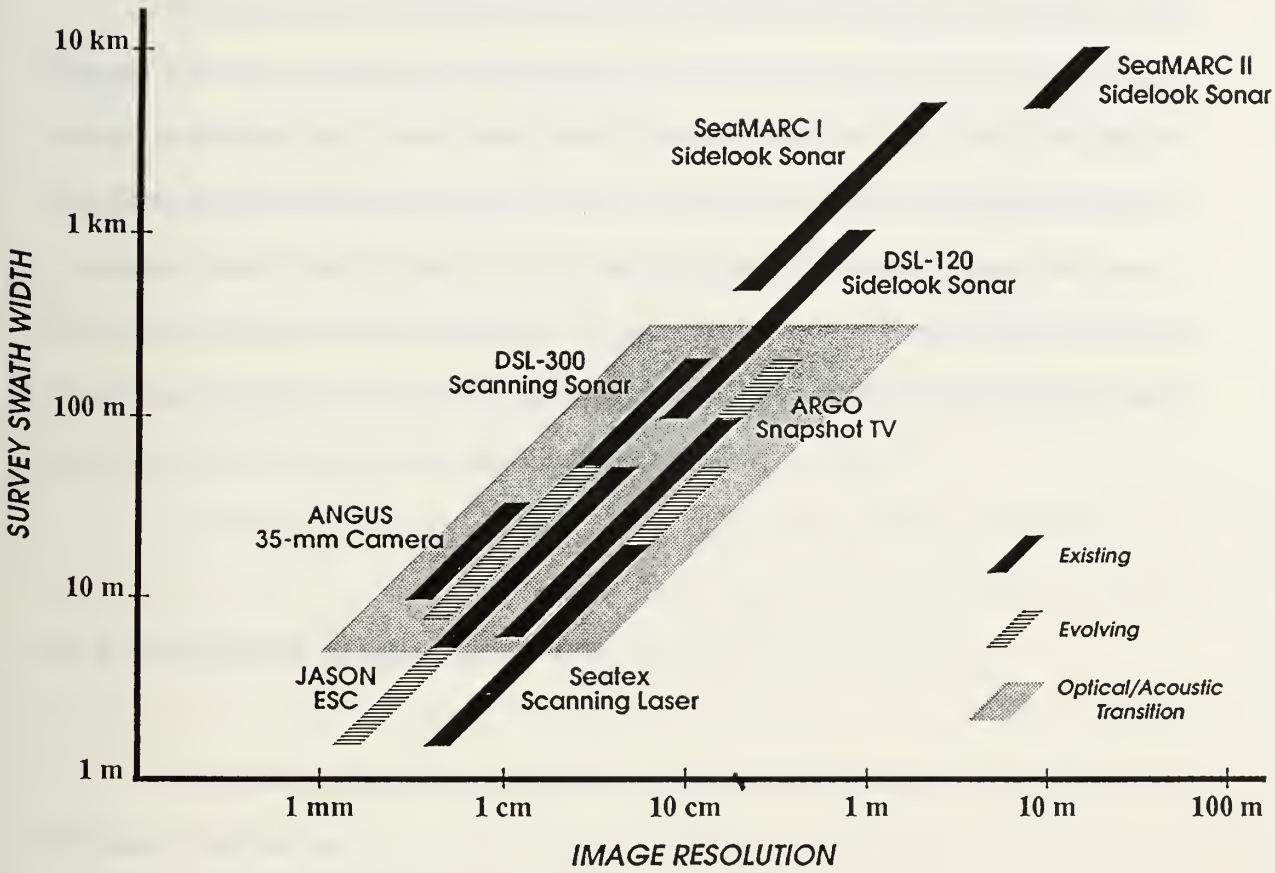

Figure 4.1 DSL comparison of underwater remote-sensing systems

- the transient nature of the displayed information, requiring the pilot to mentally integrate the overall picture.
- the inability to access the high-level, real-time environmental model.

To enhance ROV piloting efficiency, a real-time, 3-D display is envisioned. The display will access the high-level environmental model and present the user with a view closely resembling that of the video camera. Because low or medium resolution data are available prior to the ROV entering the water, a rough perspective-view display can be constructed at any time for use by the pilot on the screen previously reserved for video camera information. Such a perspective-view display is expected to be dominated in the foreground by high-resolution video data, gradually transitioning to dominance by other sensors as the limits of video range are encountered.

4.4 Targeted Human Factors

Among the myriad of potential display enhancements to improve the proposed 3-D perspective display are:

- altering the displayed field of view.
- providing a screen grid.
- displaying current range to the target of interest.
- use of a vertical color scheme.
- controlling the display update rate.

Narrowing the displayed field of view reduces the necessary graphics calculations as the square of the reduction factor. This gain must be balanced against the loss of information to the user.

Providing a 2-D or 3-D screen grid can improve the user's angular perception, provide a cross-hair effect to ease direction finding and, with the 3-D version, provide important depth cues.

Displaying current range to the target of interest can reduce the time to locate the target. This information is available in the environmental model.

Vertical color schemes are frequently used to provide redundant relief cueing for underwater and land feature presentations such as charts and maps. They can be effective in giving altitude cues for objects in the background of perspective displays.

Display update rate is limited by the data-collection cycle time of the sensors, data processing time, and graphics calculation/display time. Compromises can be made to shorten the update rate at the cost of information quality and quantity.

This thesis attempts to quantify the effects of the task-related independent variables listed above. The dependent variables for the experiments are performance time, subjective comments by the operators, and observations by the test monitor/author.

Chapter 5

Testing Display Effectiveness

5.1 Equipment

Three system hardware components were used directly by the operator: a computer monitor, a computer display, and a joystick. Other equipment transparent to the operator's task included a 386 computer with keyboard and mouse, which ran the simulation and recorded the data, and various power supply and communications cabling.

5.2 Data Point Courses

Nineteen data courses (A-R, X) were used in testing. Courses consisted of 25 sequentially numbered data points (P_j) in world coordinate system three space (x, y, z) with two constraints:

(1) Consecutive points were separated by distance $s = \sqrt{[\Delta x]^2+[\Delta y]^2+[\Delta z]^2}$, where s was a constant equal to 5 meters.

(2) A square window of given total angular width and height β, with apex at point P_j and opening in the direction of a line from P_{j-1} through P_j, contained point P_{j+1}.

Courses A, B, C and J, K, L used a 15°-square window, courses D, E, F and M, N, O used a 30° window, and courses G, H, I and P, Q, R used a 60° window. Course X, the training/familiarization course, used a 15° window. Additionally, nine of the courses were

mirror images of each other in the world coordinate system y/z plane. Mirror pairs were A/J, B/K, C/L, D/M, E/N, F/O, G/P, H/Q and I/R. Figure 5.1 and table 5.1 summarize the above information.

Visualization of each data point was provided in the form of a cubic wireframe target one meter on a side with the invisible data point at its center. Target faces were parallel to the planes formed by the world coordinate system axes. Target color was blue except for tests 5 and 6 as discussed in section 5.7. Each target was numbered with white numerals (1-25) corresponding to the sequential number of the data point at its center. A target "hit" corresponded to closing the range to the target center/data point to 0.5 meters or less from any direction. Appendix C discusses the details of target design. Appendix D contains course layout data and photographs of the courses as viewed by the operator.

Random generation of the data points for each course began with establishment of two coordinate systems, the world and the vehicle. Each system consisted of three mutually perpendicular axes x, y, and z, forming a right-hand coordinate system. The world system was fixed in space. In it, three angles were defined: ω, φ, and κ for positive rotation about the x, y and z axes respectively. Positive rotation was defined such that positive ω (φ, κ) rotated the positive y (z, x) axis into the positive z (x, y) axis through 90°. In the vehicle system, the operator was assumed to be looking down the positive y axis of the system at all times with the positive x axis to the right. Positive rotation was defined so positive θ rotated the positive y axis into the positive x axis through 90°. In this way, θ had the same sense as true heading. Figures 5.2 and 5.3 depict these systems. For a specified window width β, sets of two angles ω and κ were randomly selected from the interval $[-\beta/2, \beta/2]$. This process insured that the data points met constraint (2) above.

Based on the above coordinate system definitions, rotations of the vehicle system were broken down into individual rotations of ω, φ, and κ. Orthogonal orientation matrices were then defined for the decomposition as follows [M-2]:

$$M_\omega = \begin{bmatrix} 1 & 0 & 0 \\ 0 & \cos\omega & \sin\omega \\ 0 & -\sin\omega & \cos\omega \end{bmatrix}$$

$$M_\varphi = \begin{bmatrix} \cos\varphi & 0 & -\sin\varphi \\ 0 & 1 & 0 \\ \sin\varphi & 0 & \cos\varphi \end{bmatrix}$$

$$M_\kappa = \begin{bmatrix} \cos\kappa & \sin\kappa & 0 \\ -\sin\kappa & \cos\kappa & 0 \\ 0 & 0 & 1 \end{bmatrix}$$

The most general orientation matrix M for any combination of these three rotations was then [M-2]:

$$M = M_\omega M_\varphi M_\kappa$$

$$= \begin{bmatrix} \cos\varphi\cos\kappa & \cos\omega\sin\kappa + \sin\omega\sin\varphi\cos\kappa & \sin\omega\sin\kappa - \cos\omega\sin\varphi\cos\kappa \\ -\cos\varphi\sin\kappa & \cos\omega\cos\kappa - \sin\omega\sin\varphi\sin\kappa & \sin\omega\cos\kappa + \cos\omega\sin\varphi\sin\kappa \\ \sin\varphi & -\sin\omega\cos\varphi & \cos\omega\cos\varphi \end{bmatrix}$$

In our application pitch (ω) and yaw (κ) were allowed to vary while roll (φ) was not. The general case was then specialized by setting $\varphi = 0$ to obtain:

$$L = M_{\varphi=0} = \begin{bmatrix} \cos\kappa & \cos\omega\sin\kappa & \sin\omega\sin\kappa \\ -\sin\kappa & \cos\omega\cos\kappa & \sin\omega\cos\kappa \\ 0 & -\sin\omega & \cos\omega \end{bmatrix}$$

The matrix L_j defined the look direction from the point P_j to the next point P_{j+1} in the vehicle coordinate system. The matrix $(L_j)^*$ defined the transformation from the vehicle

coordinate system to that of the world. The origin point was taken to be $P_0 = [\ 0,0,0\ ]^T$. The first data point was taken to be $P_1 = s[\ 0,1,0\ ]^T$, where s was the constant described in constraint (1). The value (0, 0) was assigned to the set (ω, κ) at x = 0 yielding $L_0 = I_{3x3}$, the three-dimensional identity matrix, and successive L_js were generated using the above formula for matrix L and the j-th set of values (ω, κ). As a result of these specifications $(L_0)^* = I_{3x3}$ and successive $(L_j)^*$'s were calculated from the equation $(L_{j+1})^* = (L_j)^* L_j$. Successive data points were then generated using $P_{j+1} = P_j + s(L_j)^* L_j\ [\ 0,1,0\ ]^T$ as the recursive algorithm.

5.3 Modeling the Jason Vehicle

The vehicle model was a dynamic simulation of the DSL ROV Jason. The model exhibited four degrees of freedom: x (left/right), y (forward/reverse), z (up/down), and θ (CW/CCW). Hydrodynamic drag was assumed to have quadratic and linear (damping) components. Balancing forces yielded the equation (shown for the x component) :

$$(M + M_a)\,\ddot{x} + \left[\frac{(M + M_a)}{\tau_{max}}\right]\dot{x} + C_D\,\dot{x}\,|\dot{x}| = T$$

where,

M was the vehicle's mass, M_a was the vehicle's added mass, and $(M + M_a)$ was termed the vehicle's *extended mass*.

τ_{max} was a constant (2.0 s) defining the magnitude of the linear drag.

C_D was the drag coefficient.

T was the maximum thrust.

Table 5.2 summarizes the model parameters use in the experiment. Nonlinear thruster dynamics were not included in the vehicle simulation model.

The square window actually defined a portion of the surface of a sphere because point P_{j+1} was required to be exactly distance s from point P_j.

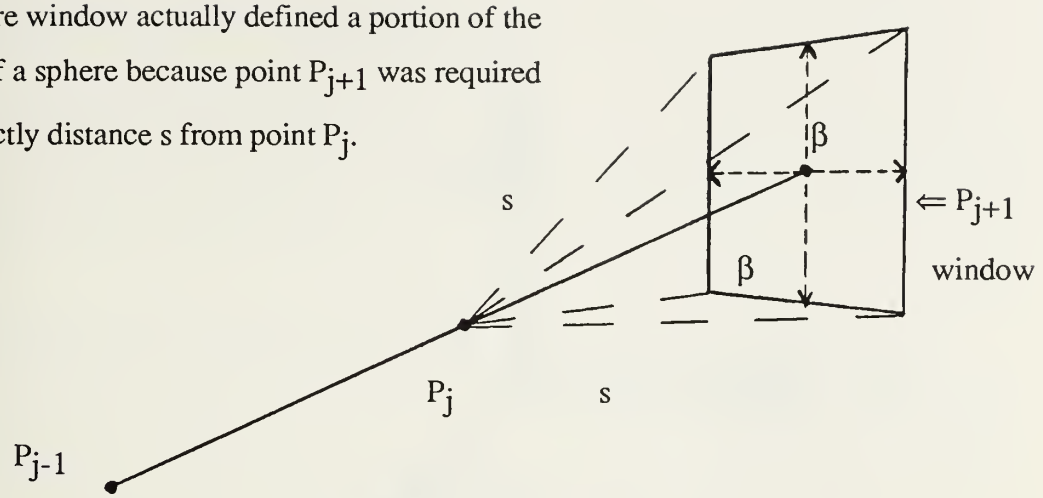

Figure 5.1 Visualization of data point course constraints

Table 5.1 Data point course relationships

	15° Solid Angle				30° Solid Angle			60° Solid Angle		
Image	A	B	C		D	E	F	G	H	I
Mirror	J	K	L		M	N	O	P	Q	R
Training				X						

Table 5.2 Dynamic vehicle simulation parameters

	Extended Mass (kg)	Drag Coefficient (kg/m or kg-m)	Max Thrust (N)	Max Velocity (m/s or rad/s)
x	1800	400	250	0.25
y	1350	350	250	0.50
z	1800	400	250	0.25
θ	450	250	41.5	0.157

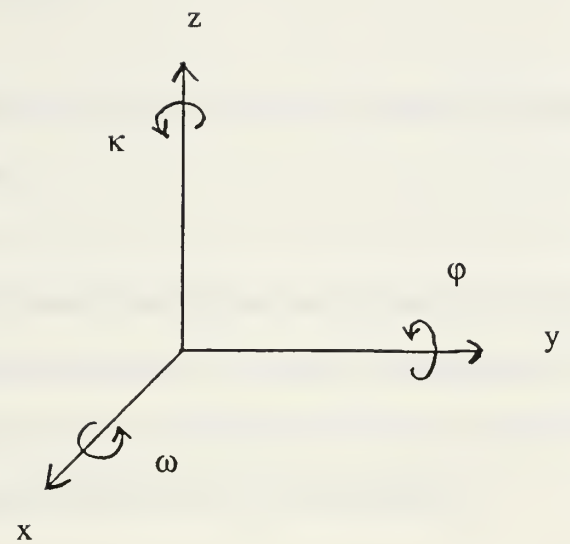

Figure 5.2 The world coordinate system

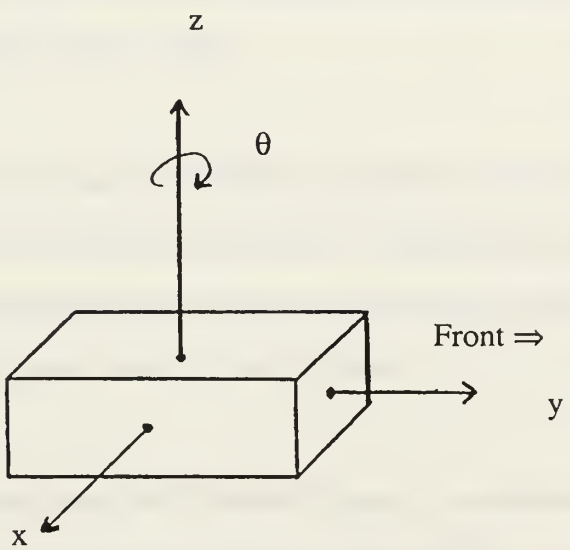

Figure 5.3 The vehicle coordinate system

5.4 Operators and Training

The same four operators were used in each of the seven tests. The author was not an operator. Operator profiles were:

Operator I was a 22 year old, male Naval Officer and graduate student with uncorrected full visual acuity and normal color vision. This right-handed subject had frequently played video games including flight simulators. He was familiar with 3-D perspective computer displays prior to the experiment.

Operator II was a 24 year old, male graduate student with uncorrected full visual acuity and normal color vision. This left-handed subject had little exposure to video games such as flight simulators. He was familiar with 3-D perspective computer displays prior to the experiment due to practical experience with computer systems as an undergraduate Computer Science major.

Operator III was a 34 year old, male Naval Officer and graduate student with uncorrected full visual acuity and normal color vision. This right-handed subject had some exposure to video games such as flight simulators. He was familiar with 3-D perspective computer displays prior to the experiment.

Operator IV was a 32 year old male with a Master's Degree, uncorrected full visual acuity, and normal color vision. This right-handed subject had little exposure to video games such as flight simulators. He was not familiar with 3-D perspective computer displays prior to the experiment.

Prior to each testing session, operators were briefed in the following areas:

general, simulation, and hardware. The general topics included purpose of thesis and experimental approach, time measurement, and operator errors. Simulation topics included target and course design as well as vehicle modeling. Hardware subjects discussed important features of the computer monitor, the computer display, and the joystick. Additionally, a maximum of 15 minutes was allotted for familiarity training with a 60°, 30°, or 15° field of view, as appropriate to the test, using training course X.

The tests were conducted in a total of four separate sittings to reduce operator fatigue. Test 1 (see number designations below) was conducted alone. The remaining tests were conducted in pairs in the following order: 2/3, 4/5, and 6/7.

5.5 Test 1 - Field of View

Testing for field of view measured changes in the operator's spatial performance versus the displayed field of view.

Test 1 description: All targets were colored blue. The operators drove the simulated vehicle point to point over a course of 25 data points spaced in x, y, and z. Operators completed nine courses, each varying in x/y/z with a maximum 15°, 30°, or 60° spread in data from point to point. Measured fields of view were 15°, 30°, and 60°. The display update period was fixed at two seconds. Nine combinations of FOV and courses were used with each of the four operators.

5.6 Tests 2 and 3 - Gridding

Testing for gridding measured the improvement in operator performance when

presented with a visual reference grid in the display.

Test 2 description: All targets were colored blue. The operators drove the simulated vehicle point to point over a course of 25 data points spaced in x, y, and z. Operators completed three courses, each varying in x/y/z with a maximum 15°, 30°, or 60° spread in data from point to point. The field of view was fixed at 60° and the display update period at two seconds. A two-dimensional (2-D) grid was superimposed on the visual display.

Test 3 description: All targets were colored blue. The operators drove the simulated vehicle point to point over a course of 25 data points spaced in x, y, and z. Operators completed three courses, each varying in x/y/z with a maximum 15°, 30°, or 60° spread in data from point to point. The field of view was fixed at 60° and the display update period at two seconds. A three-dimensional (3-D) grid was superimposed on the visual display.

5.7 Tests 4 and 5 - Vertical Color Schemes

Testing for color scheme measured the improvement in operator performance using a fixed, vertical-relief color scheme for target shading versus single-color targets. The 6-color set provided 12 meter vertical color swaths while the 21-color set provided three meter vertical color swaths over the range of interest. Table 5.3 lists the color sets.

Test 4 description: Targets were shaded in color according to height z above ocean floor. The color scheme was divided into six discrete shades. The operators drove the simulated vehicle point to point over a course of 25 data points spaced in x, y, and z. Operators completed three courses, each varying in x/y/z with a maximum 15°, 30°, or 60° spread in

Table 5.3 The color sets (1, 6, 21) and associated altitude bands

Set	Target	Color	Red	Green	Blue	Z value (meters)
1	0	Blue	0	0	1	All
6	1	Red	1	0	0	< 88
6	2	Yellow	1	1	0	76 - 88
6	3	Green	0	1	0	64 - 76
6	4	Cyan	0	1	1	52 - 64
6	5	Blue	0	0	1	40 - 52
6	6	Magenta	1	0	1	< 40
21	7	Red	1	0	0	> 93
21	8	Reddish Orange	1	0.25	0	90 - 93
21	9	Orange	1	0.50	0	87 - 90
21	10	Yellowish Orange	1	0.75	0	84 - 87
21	11	Yellow	1	1	0	81 - 84
21	12	Yellowish Yellow-Green	0.75	1	0	78 - 81
21	13	Yellow-Green	0.50	1	0	75 - 78
21	14	Greenish Yellow-Green	0.25	1	0	72 - 75
21	15	Green	0	1	0	69 - 72
21	16	Greenish Aquamarine	0	1	0.25	66 - 69
21	17	Aquamarine	0	1	0.50	63 - 66
21	18	Cyanish Aquamarine	0	1	0.75	60 - 63
21	19	Cyan	0	1	1	57 - 60
21	20	Cyanish Turquoise	0	0.75	1	54 - 57
21	21	Turquoise	0	0.50	1	51 - 54
21	22	Blueish Turquoise	0	0.25	1	48 - 51
21	23	Blue	0	0	1	45 - 48
21	24	Blueish Purple	0.25	0	1	42 - 45
21	25	Purple	0.50	0	1	39 - 42
21	26	Magentaish Purple	0.75	0	1	36 - 39
21	27	Magenta	1	0	1	< 36

data from point to point. The field of view was fixed at 60° and the display update period at two seconds.

Test 5 description: Targets were shaded in color according to height z above ocean floor. The color scheme was divided into 21 discrete shades. The operators drove the simulated vehicle point to point over a course of 25 data points spaced in x, y, and z. Operators completed three courses, each varying in x/y/z with a maximum 15°, 30°, or 60° spread in data from point to point. The field of view was fixed at 60° and the display update period at two seconds.

5.8 Test 6 - Heads Up Range

Testing for range measured the improvement in operator performance when presented with continuously revised range to target center information.

Test 6 description: All targets were colored blue. The operators drove the simulated vehicle point to point over a course of 25 data points spaced in x, y, and z. Operators completed three courses, each varying in x/y/z with a maximum 15°, 30°, or 60° spread in data from point to point. The field of view was fixed at 60° and the display update period at two seconds. Continuously revised range to target center was provided to the operator.

5.9 Test 7 - Display Update Rate

Testing for display update rate measured the degradation in operator performance associated with reduced visual information feedback.

Test 7 description: All targets were colored blue. The operators drove the simulated vehicle point to point over a course of 25 data points spaced in x, y, and z. Operators completed three courses, each varying in x/y/z with a maximum 15°, 30°, or 60° spread in data from point to point. The field of view was fixed at 60°. The display update period was slowed to four seconds.

Chapter 6

Testing Results

6.1 General

The first step in the analysis was to convert the logged target hit times into time differences between successive targets. Appendix E lists the resultant time differences. The second step was normalize the raw data from Appendix E by removing the effects properly attributed to variations in the level of course difficulty related to the Jason vehicle simulation model. This procedure divided each time difference (in seconds) by the best time (in seconds) that could be made between the associated targets based on the vehicle simulation. Appendix D discusses the method of arriving at this best time between targets and lists those times in table form. Appendix F contains the normalized, dimensionless values. The third step was to estimate the operators' learning curves to standardize results between tests. These results were then analyzed directly to assess the effectiveness of the tested display enhancements.

6.2 Operator Learning Curves

Operator learning reflected a number of factors including increasing familiarity with test equipment, improving knowledge of test procedures, and gradual easing of pretest anxiety, as well as modified strategies for driving the simulated vehicle. Estimation of the

operators' learning curves involved four assumptions.

- The learning curves had positive slope at all times. This meant that the operators were constantly improving with no loss of knowledge or acquired skills between testing sessions.
- The learning curves were smooth functions. This prohibited the consideration of learning plateaus during which operators would show no improvement.
- The learning curves were exponential functions.
- For a specified field of view, operator learning was reflected primarily in the standard deviation of the normalized course times (a smoothness measure). The effectiveness of display enhancements was reflected primarily in the total course times (a measure of speed).

As an additional consideration, test 1 was designed to force the operators to use a variety of strategies, particularly with the reduced fields of view, in an attempt to ensure maximum learning in minimum time.

Each operator drove 21 courses with a 60° field of view, three for each of the seven tests. The procedure below was applied to the normalized data for each operator to estimate his 60° FOV learning curve.

- The standard deviations were entered into a 3 x 7 matrix. Each row represented a specific window width β as discussed in section 5.2 (row 1 = 15°, row 2 = 30°, and row 3 = 60°). Each column corresponded to a given test (column 1 = test 1, column 2 = test 2, etc.).
- The standard deviations for the three window widths for each test were summed and entered into a row vector of seven elements. Each column continued to represent a given test as above. This step yielded the summed standard deviations (SSD) shown in table 6.1.
- The row vector elements were plotted with summed standard deviations on the vertical axis versus test number on the horizontal axis.

- An exponential curve using the method of least squares was fitted to the plot by linearizing the exponential form through taking logarithms [G-1]. This defined the operator's learning curve. Appendix G shows the graphed operators' learning curves.

Once the operators' learning curves were estimated, correction factors to allow results between tests to be compared were derived using the following procedure.

- Estimated standard deviation values were extracted from the fitted exponential curve using regression techniques. This step produced the extracted values (EV) listed in table 6.1.
- Standardization factors (SF) were formed by dividing all EVs by the first (and largest) value. The EVs are listed in table 6.1.
- The 84 mean values of the normalized 60° FOV course times listed in Appendix F were multiplied by the associated SF. This step resulted in the learning-corrected, normalized mean times (LCNMT) listed in table 6.2.
- For each test, the LCNMTs for all operators were summed. The mean and standard deviation of each LCNMT sum were found, completing the data manipulation.

Figure 6.1 shows the plotted means and standard deviations of the normalized mean times without correction for individual operator learning curves. Figure 6.2 shows the means and standard deviations of the LCNMT sum plotted for analysis.

The learning curve for the different fields of view could not be estimated using the same techniques. It was assumed that the individual operator's 60° FOV learning curve was a good approximation and the first three SFs from table 6.1 for each operator were applied to the data.

Table 6.1 Summed standard deviations (SSD), extracted values (EV), and standardization factors (SF)

	Operator I			Operator II			Operator III			Operator IV		
Test	SSD	EV	SF	SSD	EV	SF	SSD	EV	SF	SSD	EV	SF
1	4.16	3.56	1.00	7.65	5.86	1.00	7.35	5.32	1.00	3.85	3.51	1.00
2	3.01	3.39	1.05	5.55	5.12	1.15	3.72	5.01	1.06	3.09	3.48	1.01
3	3.36	3.22	1.11	4.41	4.47	1.31	5.70	4.71	1.13	3.48	3.46	1.01
4	2.73	3.06	1.17	2.36	3.90	1.50	3.47	4.43	1.20	3.20	3.43	1.02
5	2.75	2.91	1.23	2.66	3.40	1.72	3.45	4.17	1.28	3.59	3.41	1.03
6	2.53	2.76	1.29	3.31	2.97	1.97	3.82	3.92	1.36	3.67	3.38	1.04
7	3.10	2.62	1.36	3.56	2.59	2.26	4.82	3.69	1.44	3.20	3.36	1.04

Table 6.2 Learning-corrected, normalized mean times (60° FOV)

	Operator I			Operator II			Operator III			Operator IV		
Test	15° β	30° β	60° β	15° β	30° β	60° β	15° β	30° β	60° β	15° β	30° β	60° β
1	1.84	2.26	3.62	3.00	2.90	5.55	2.52	3.32	3.85	3.70	3.15	3.48
2	2.18	2.38	3.65	2.10	3.47	4.72	2.91	2.32	3.77	2.18	1.93	3.03
3	1.90	1.85	3.26	3.49	4.12	4.65	3.09	3.26	2.81	1.61	1.94	2.95
4	1.71	1.94	3.09	2.31	2.68	4.57	2.74	2.20	4.20	1.98	1.81	3.11
5	2.65	2.02	3.43	3.23	3.68	4.78	2.98	2.69	3.11	1.61	1.56	2.93
6	1.81	2.40	3.61	3.94	3.67	7.77	2.12	4.02	4.68	1.66	2.40	3.14
7	2.71	3.60	3.97	6.33	5.87	7.81	3.58	4.66	5.63	2.06	2.20	3.40

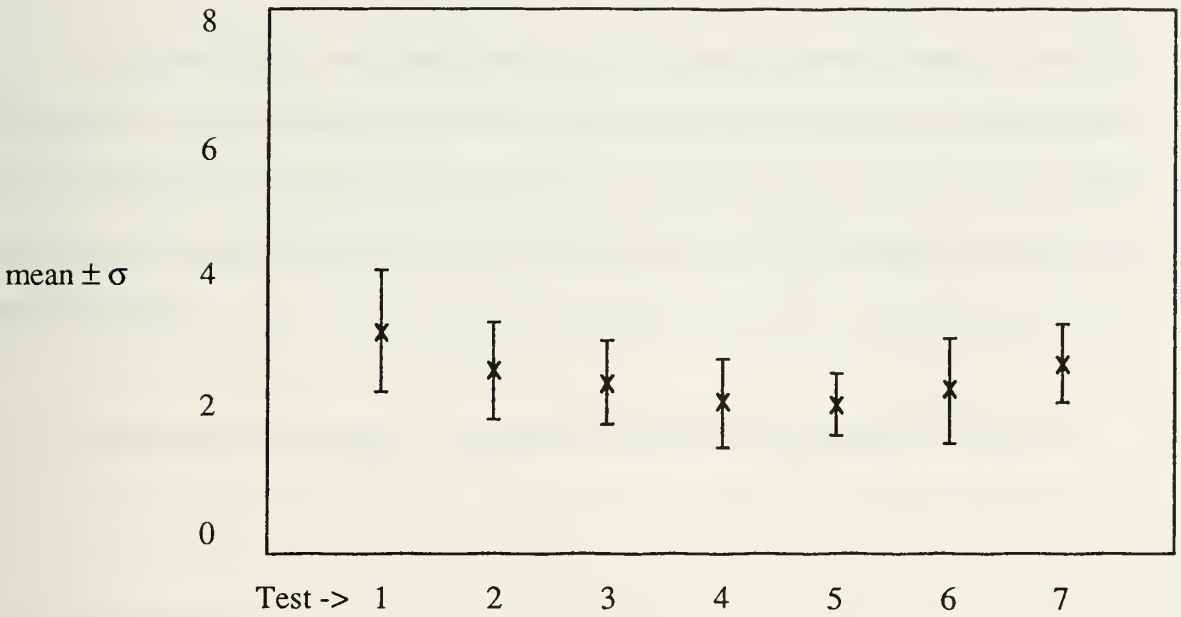

Figure 6.1 Normalized mean times (60° FOV)

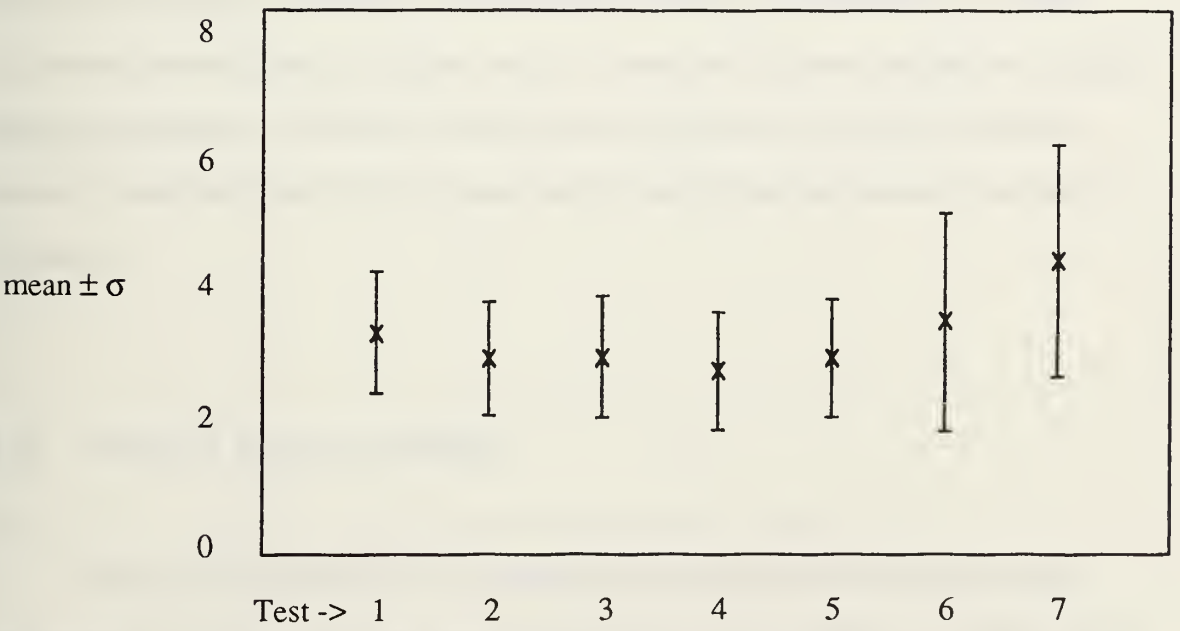

Figure 6.2 Learning-corrected, normalized mean times (60° FOV)

6.3 Field of View

The three fields of view used in testing were related by inverse powers of two (60°, 30°, and 15°). Plotted means and standard deviations of the learning-curve-corrected data versus FOV scaled by inverse powers of two were virtually linear and clearly demonstrated the parabolic relationship between the mean run time and the FOV. Fitting a parabola to the data showed that:

$$\text{normalized mean run time} = 10.399 - 0.200 * FOV + 1.350 * 10^{-3} * FOV^2.$$

6.4 Gridding

The 2-D and 3-D grids improved operator performance to the same degree (34.64 and 34.92 respectively). The 2-D grid was simple and straightforward to employ. The 3-D grid conveyed more information, but cluttered the display and was harder to interpret. The primary benefit of the 2-D display was the "cross-hairs" effect of the grid, which aided steering effectiveness. This effect was less pronounced with the 3-D grid. Hidden-line removal, particularly for a 3-D grid, could provide strong visual range cues in the vicinity of a target.

6.5 Vertical Color Schemes

The 6-color scheme and the 21-color scheme both provided improved operator performance. The 6-color scheme proved to be slightly better (32.34 versus 34.68). This effect was attributed to its simplicity and the high-contrast, easily distinguished colors. The

Table 6.3 Learning-corrected, normalized mean times (varying FOV)

	Operator I			Operator II			Operator III			Operator IV		
FOV	15° β	30° β	60° β	15° β	30° β	60° β	15° β	30° β	60° β	15° β	30° β	60° β
60	1.84	2.26	3.62	3.00	2.90	5.55	2.52	3.32	3.85	3.70	3.15	3.48
30	5.89	5.07	4.99	4.63	4.73	6.05	6.49	5.71	7.13	3.80	4.11	8.83
15	5.97	4.96	7.17	7.30	10.7	11.6	2.28	5.63	11.1	6.75	8.45	10.5

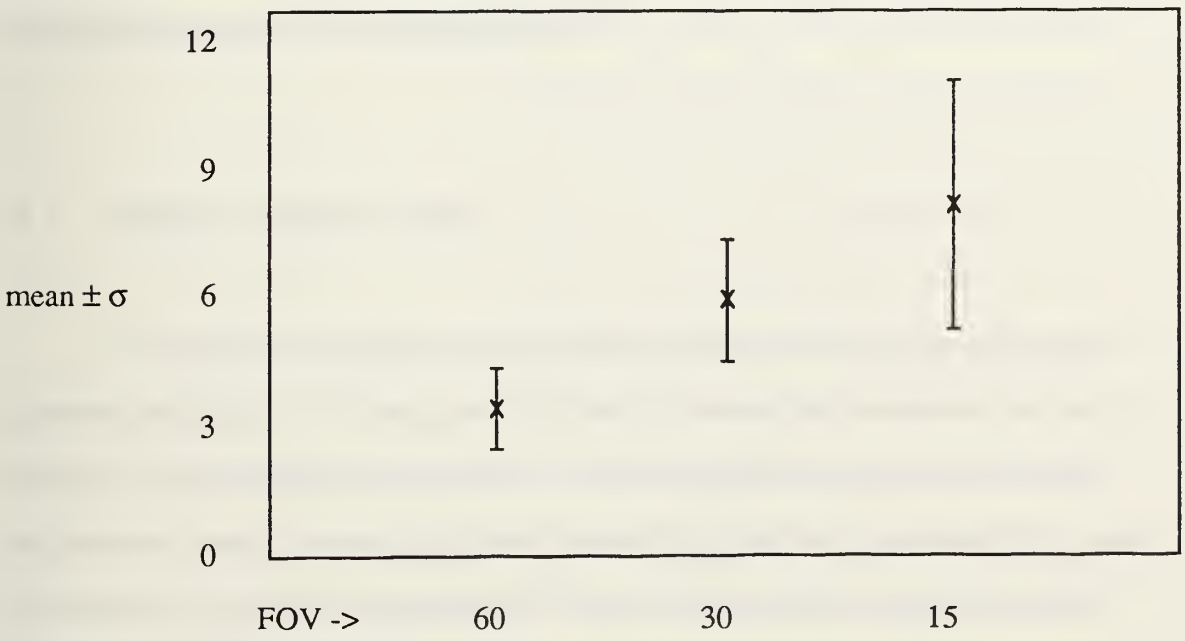

Figure 6.3 Learning-corrected, normalized mean times (varying FOV)

primary benefit of the color schemes was improved spatial perception of the display due to the combined effects of depth and altitude cues. These two cues were strongly interrelated.

6.6 Heads-Up Range

A surprising result was the degradation of operator performance when supplied with range to the target center. Although the range information proved valuable if a target was not visible, was close, or had been missed, this was more than offset by negative factors. Primary problems included ignoring the visual information of the display and the "perigee effect," where a control action that caused the range to initially decrease would not necessarily result in a hit. As the vehicle's trajectory passed perigee with the target's center, the range increased, frequently confusing the operator. No individual operator's performance improved with range information.

6.7 Display Update Rate

As anticipated, slowing the graphics display update rate by a factor of two hurt operator performance. The magnitude of this effect, slowing the normalized run time by a factor of 1.3, was smaller than anticipated. This had significant implications for field applications, where a longer update period would allow the use of less powerful computer equipment or more robust programming. The loss of the operator's ability to mentally integrate the visual information from the display and use kinetic depth-effect cues was mitigated by the more conservative driving approach adopted by the operators. All the operators demonstrated this slowing effect with update rate.

6.8 Operator Comments

Relevant operator comments were broken down into the categories of field of view, grids, color sets, range data, update rate, test equipment, test design, and strategy (operator number is included in parentheses after comments).

- Field of View- Narrowing the field of view placed a premium on maintaining visual contact with the targets (II).
- Grids - The "cross-hairs" effect aided steering effectiveness (II, IV).

  Grids provided relative size information (II).

  The 3-D grid was more intuitive and effective than the 2-D grid (II).

  The 3-D grid cluttered the display (IV).

  The grids were not particularly helpful (III).

  Hidden-line removal for grids could provide strong visual range cues in the immediate vicinity of a target by showing the target "poking through" the grid (I, IV).

  The black grids were sometimes confused with the blue targets when the display was cluttered (IV).

  The operator's need for a grid was reduced by improvements in his spatial perception (IV).
- Color Sets - Color provided spatial visualization cues, especially with overlapping targets (all).

  The 21-color set provided significantly more information and was more effective than the 6-color set (II, IV).

  Color information was far superior to gridding (III).

  Target course altitude slope information was available from the rate of change of target colors (III).

A sliding color scale with the vehicle always at scale center could provide improved relative altitude cues (III).

- Range Data - Range information proved valuable if a target was not visible, was close, or had been missed (all).

  Range information was ignored if a target was in view (II).

  Range information provided for smoother driving near targets and eased hitting targets off-center (II, IV).

  The operator perceived that targets were "hit" from a greater distance with range information available (III).

- Update Rate - Operators drove more conservatively with the slower update rate (II, III).

  Update rate was more important as the range decreased (III).

  Vehicle alignment with the target trend was more important with the slower update rate due to the time lag in update rate while rotating (IV).

  Operator workload increased with slower update rate (I).

  The slow update rate was not as difficult as anticipated (IV).

- Test Equipment - The joystick was very tiring to use, particularly the z-axis pure-force control (III).

  Fine z-axis movement was difficult due to the stiff pure-force control (II, III).

  Axis movement with the joystick was not compatible with operator expectations (I, III).

  Presentation of all information on one screen could ease operator workload (all).

- Test Design - Target drawing order proved confusing (I, II, III).

  The display graphics can be cluttered, particularly with a

narrow field of view (I, II, III).

The simulated vehicle lacked an effective altitude search capability (I, III).

Operator efficiency was reduced by the fixed 2-D target numbers when approaching targets from the side (all).

Improved heading perception was provided by the fixed 2-D target numbers (II).

- Strategy - Operator comfort with vehicle rotation improved as testing progressed (I, III).

Operators needed to plan more than one target in advance and, when possible, kept them on the display (II, III).

Rotating the vehicle to line up along the target heading trend reduced the time between targets (II, III).

Knowledge of the course trend aided target identification (IV).

Driving while backing up was counterintuitive (III).

6.9 Test-Monitor Observations

Test-monitor observations not previously listed under operator comments were broken down into the categories of color sets, range data, update rate, test equipment, test design, strategy, and tendencies.

- Color Sets - Some colors were weak in contrast with the background

dark gray. Reddish Orange and Turquoise were most difficult for the operators to discern.

- Range Data - Range information sometimes handicapped the operators by providing too much data, causing them to ignore the display visual information. Another detrimental effect was that a control action that caused the range to initially decrease would not necessarily result in a hit. As the vehicle's trajectory passed perigee with the target's center, the range would increase. This effect fooled all operators initially, particularly when moving the vehicle along more than one axis simultaneously.
- Update Rate - The four-second update period significantly degraded the operator's ability to mentally integrate the display information and use kinetic depth-effect cues.
- Test Equipment - Stiffness of the joystick resulted in unorthodox grips being employed, many with both hands.
- Test Design - An artifact of the wireframe target design was that the simulated vehicle could be close to or within the target without any portion of the target being visible on the display. This is an unlikely scenario in the field.
- Strategy - Backing up to keep the previous target in view while looking for the next target was an effective approach when presented with a limited field of view.

  Heading information was underutilized. Two possible uses were to measure the target trend heading and align

the vehicle accordingly, and to improve the general sense of spatial orientation of the operator.

Operators adopted differing strategies for driving. These strategies were modified during testing but did not converge to a single "correct" method.

An effective search technique when no target was in view was critical in reducing course run time.

"Crabbing" or twisting one direction while moving side to side in the opposite direction was effective in realigning with a new course heading trend while keeping targets in view.

- Tendencies - Applying excessive control actions and failing to account for the delay caused by the update rate was a problem, especially when in close proximity to a target.

Operators were hesitant to identify target numbers when only a portion of the number was visible or the angle of view approached 90°.

As testing progressed, the operators became more confident in controlling the vehicle in two or three directions simultaneously.

Operators occasionally applied the correct axis-control order in the opposite direction from that intended. This was related to the well-known outside-in versus inside-out viewing problem.

Operator average velocities increased as familiarity with the testing improved.

Chapter 7

Summary, Conclusions and Recommendations

7.1 Summary

Effective collection, computation, and presentation of undersea data to the ROV pilot on a single screen presents hardware, software and human-factors problems. Pilot performance efficiency through improved display design is a key human factors issue. Seven tests measured the effects of an enhanced 3-D perspective display on the simulated piloting of an ROV. The effects of the ROV simulation and operator learning curves were removed to directly compare performance changes due to the various enhancements.

7.2 Conclusions

Display enhancements that improved operator performance were:

- widening the field of view.
- providing a gridded screen reference.
- using vertical color schemes to cue depth/altitude information.
- shortening the display update period.

The singularly most important factor for the operator was widening the field of view. Providing the operator with continuous range information to the target center

degraded performance.

Many operator comments carried strong implications for system design.

- The "cross-hairs" effect of a grid aided steering effectiveness.
- Hidden-line removal for grids could provide strong visual-range cues in the immediate vicinity of a target by showing the target "poking through" the grid.
- Color provided spatial visualization cues and altitude slope information.
- Range information proved valuable if a target was not visible, was close, or had been missed.
- The update rate was more important as the range decreased.
- The joystick was very tiring to use. Fine z-axis movement was difficult due to the stiff pure-force control.
- Presentation of all information on one screen could ease operator workload.

Several operator comments were not supported by the test results.

- The 3-D grid was not more effective than the 2-D grid. They were nearly identical in overall effectiveness.
- The color schemes were not far superior to the grids. The difference between the 2-D grid, the 3-D grid, and the 21-color scheme was insignificant. The 6 color scheme was only slightly better.
- The 21-color set was not more effective than the 6-color set.

Several significant improvements to the proposed 3-D perspective display are available through incorporation of the best features of the display enhancements tested. A single screen with as wide a field of view as possible and limited distortion, a cross-hair, a simple vertical color scheme, target range information, and a reasonable update period (two

seconds or less) would improve ROV pilot effectiveness. More testing would be necessary to determine the best design for a 2-D or 3-D grid. The key to effective use of range information is the method of employment.

7.3 Recommendations

This thesis investigated the effects of individual display enhancements on operator performance. In order to take maximum advantage of the positive aspects that each of the enhancement has to offer, several need to be implemented simultaneously. Due to the potentially complex nature of the enhancement interactions, it is unwise to generalize the individual results into group results. These interactions need to be analyzed on a case basis.

The presentation of both printed information such as position and velocities as well as graphics on the same screen was recommended by all operators. This capability exists in modern computer windowing environments. The effectiveness of any proposed screen layout design requires both qualitative and quantitative assessment.

One operator commented that a sliding color scale with the vehicle always at scale center could provide improved relative-altitude cues. This suggestion has merit and bears further investigation.

Both operators and pilots expressed strong dissatisfaction with the Measurement Systems, Inc., joystick designs (fourth-axis control by lifting/depressing the stick vertically or pure-force button). The sticks are far too difficult to use for extended periods due to their bulk, stiffness, and awkward incorporation of fourth-axis control. Catalog search has yet to produce a fully acceptable alternative, although a different joystick model is currently in use. Pilot preferences indicate that a modified video-game joystick is closer to their concept of an acceptable control. Identification of design requirements, development,

testing to ensure effectiveness, and procurement of a fully acceptable control is an area needing attention.

Between testing sessions, usually a day or two apart, operators experienced a decay of previously acquired skills. The driving of course X prior to each test appeared to reverse this decay. ROV piloting is not a full-time occupation. Frequently months pass between cruises. Pilots also change employers, reducing the corporate piloting knowledge level. Three actions are recommended to reduce this loss of skills:

- Holding precruise pilot discussions to reawaken piloting skills. Critical to these discussions would be the minutes of the previous post-cruise debriefs.
- Conduct of precruise pilot simulator training. Construction of a simulator with the field equipment would be straightforward and all the necessary hardware is already in hand. Pilot discussions of strategies could be demonstrated and tested prior to use in the field. Added benefits of a simulator include serving as a test bed for new display designs and the ability to write the simulator software to incorporate precruise system checks.
- Holding postcruise debriefs to document problems, fixes, and strategies. The minutes of these debriefs would generate a valuable storehouse of piloting knowledge.

APPENDIX A

Nomenclature

Symbol	Meaning	Units	Page
C_D	coefficient of drag	kg/m or kg-m	38
L_j	look direction matrix from point P_j to point P_{j+1} in vehicle system	none	37
$(L_j)^*$	transformation matrix from vehicle system to world system	none	37
M	vehicle mass	kg	38
M_a	vehicle added mass	kg	38
M_κ	rotation matrix for κ angular rotation	none	37
M_φ	rotation matrix for φ angular rotation	none	37
M_ω	rotation matrix for ω angular rotation	none	37
P_j	j-th data point	none	35
T	maximum thrust	N	38
β	operator field of view angular width	rad	35
θ	vehicle system rotation angle about z axis	rad	26
κ	world system rotation angle about z axis	rad	36
σ	standard deviation	none	51
τ_{max}	linear drag (damping) coefficient	s	38
φ	world system rotation angle about y axis	rad	36
ω	world system rotation angle about x axis	rad	36

kg	kilograms
m	meters
N	newtons
rad	radians
s	seconds

APPENDIX B

Abbreviations

Symbol	Meaning	Page
ACM	Association for Computing Machinery	133
BBN	Bolt, Beranek, and Newman	23
CCW	Counterclockwise	38
CDR	Commander	3
CIE	Commission Internationale de l'Eclairage	19
CRT	Cathode Ray Tube	13
CW	Clockwise	38
DSL	Deep Submergence Laboratory	8
DV	Dependent Variable	22
EV	Extracted Value	10
FJCC	Fall Joint Computer Congress	134
FOV	Field of View	8
GDM	Graphic Display Monitor	27
HOOPS	Hierarchical Object Oriented Picture System	25
HSB	Hue, Saturation, and Brightness	10
IEEE	Institute of Electrical and Electronics Engineers	133
IFIP	International Federation for Information Processing	134
ISCC-NBS	Inter-Society Color Council - National Bureau of Standards	19
IV	Independent Variable	22
LCDR	Lieutenant Commander	136

LCNMT	Learning-Corrected, Normalized Mean Times	49
MIPS	Millions of Instructions Per Second	26
MIT	Massachusetts Institute of Technology	1
MFLOPS	Millions of Floating-Point Operations Per Second	26
N/A	Not Applicable	73
NEC	Nippon Electric Company	27
NTSC	National Television System Committee	26
RGB	Red, Green, Blue	8
ROV	Remotely Operated Vehicle	2
SF	Standardization Factor	10
SHARPS	Sonic High Accuracy Ranging and Positioning System	31
SONAR	Sound Navigation and Ranging	2
SSD	Summed Standard Deviation	10
TI	Texas Instruments	23
UCL	Universal Color Language	19
USN	United States Navy	3
VCR	Video Cassette Recorder	26
VGA	Video Graphics Adapter	27
WHOI	Woods Hole Oceanographic Institution	1
YIQ	Luminance, In-phase, and Quadrature	19
2-D	Two-Dimensional	8
3-D	Three-Dimensional	2

APPENDIX C

Target and Grid Design

All seven tests used the same 25 cubic-wireframe targets. Each target was one meter on a side with the invisible x, y, and z data point at its center. Target faces were parallel to the planes formed by the world coordinate system axes. Target colors were blue except for tests 5 and 6 as discussed in section 5.7. Each target was numbered with white numerals (1-25) corresponding to the sequential number of the data point at its center. The numbers were 2-D wireframes 0.5 meters in height, 0.3 meters in width (numeral one was 0.1 meters in width), and drawn parallel to the XZ world coordinate plane facing the initial position of the vehicle. All numbers were drawn centered in the target in the x, y, and z directions.

Embedded in each target was an invisible sphere of one-meter diameter. This sphere defined the "hit" criterion for its target. When the vehicle, modeled as a point, touched the sphere, the target was hit. This corresponded to closing the range to the target center to 0.5 meters or less from any direction.

The 2-D grid used in test 2 was composed of 16 black squares arranged in four rows of four. The grid was drawn centered, parallel to, and aligned with the edges of the display face at a screen depth of five meters. Each square was scaled so it was one meter on a side at that depth. Figure C.1 shows the operator's display of the 2-D grid with target course X.

The 3-D grid used in test 3 was composed of 200 black squares and rectangles arranged in three panels. The center panel was made up of 100 squares in 10 rows of 10. This grid was drawn centered, parallel to, and aligned with the edges of the display face at a screen depth of five meters. Each square was scaled so that it was 0.25 meter on a side at

that depth. The side panels were each made up of 50 rectangles in 10 rows of five. Each rectangle was 0.25 meter in height and one meter in width. The side panels were attached to the center grid at right angles to its left and right edges. The assembled grid formed a box with no top or bottom facing the operator. Figure C.2 shows the operator's display of the 3-D grid with target course X.

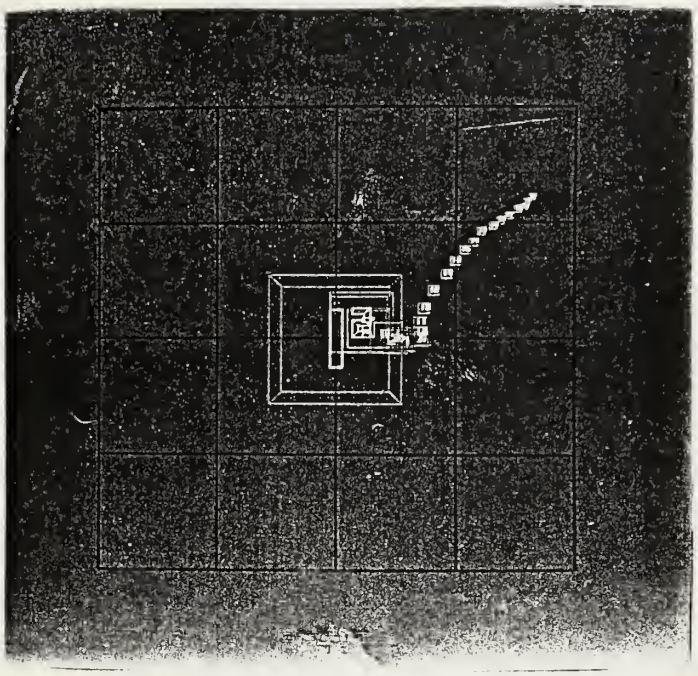

Figure C.1 2-D grid (operator's display with 60° FOV and target course X)

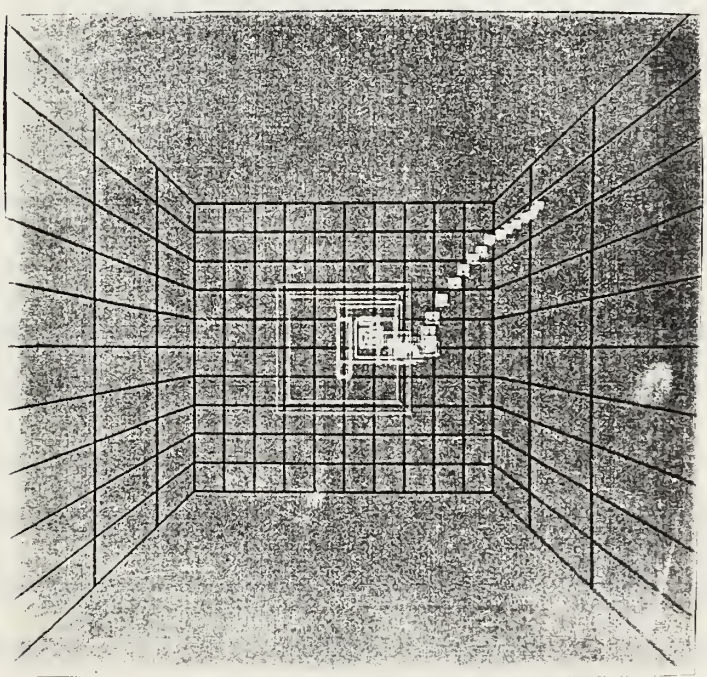

Figure C.2 3-D grid (operator's display with 60° FOV and target course X)

APPENDIX D

Data Point Courses

Tables D.1 through D.19 list the x, y, and z positions of the centers of targets 1 through 25 for each of the target courses. The method for generating these x, y, and z positions is discussed in detail in section 5.2. Additionally, the shortest time difference (best δt) between the centers of successive targets is listed for courses A through R. The best δt between targets U and V was calculated as follows:

- altitude distance from z_u to z_v was calculated, then divided by the best up/down speed (0.25 m/s), resulting in the best up/down time.
- the change in vehicle heading at target U to fly directly to target V was noted.
- distance in the horizontal plane from (x_u , y_u) to (x_v , y_v) was calculated.
- this horizontal distance was decomposed into forward and lateral components based on the vehicle's heading prior to reaching target U.
- the decomposed forward distance was divided by the best forward speed (0.5 m/s).
- the decomposed lateral distance was divided by the best lateral speed (0.25 m/s).
- the minimum time to travel the horizontal distance without heading change was the larger of the best forward and lateral speed times.
- vehicle heading change was divided by the best rotational velocity (0.157 rad/s).
- the total horizontal distance was divided by the best forward speed (0.5 m/s).
- the minimum time to travel the horizontal distance with heading change was the sum of the best rotational velocity time and the best forward speed time.
- the minimum time to travel the horizontal distance was the smaller of the times with and without heading change.

- the best time between targets was the larger of the best up/down and horizontal times.

Figures D.1 through D.18 were reproduced from photographs of the operator's initial display for courses A through R with a 60° field of view. Figures D.19, D.20, and D.21 were reproductions of the initial display for course X with a 60°, 30°, and 15° field of view respectively.

Table D.1 Course A

Target	x	y	z	Best δt
1	75	5	50	N/A
2	75.340	9.971	50.419	9.942
3	75.683	14.959	50.393	10.000
4	75.743	19.937	50.862	9.940
5	76.337	24.897	51.060	9.935
6	77.204	29.809	50.703	9.959
7	78.401	34.662	50.821	9.975
8	79.848	39.447	50.718	9.984
9	80.992	44.314	50.665	9.980
10	82.121	49.184	50.707	10.000
11	83.810	53.888	50.570	9.928
12	86.077	58.330	50.930	9.894
13	88.094	62.885	51.366	9.947
14	90.093	67.411	52.085	9.896
15	91.666	72.019	53.219	9.704
16	92.761	76.807	54.158	9.770
17	93.676	81.488	55.659	9.536
18	94.076	86.374	56.640	9.742
19	94.950	91.283	57.016	9.935
20	95.347	96.261	57.262	9.940
21	95.595	101.250	57.047	9.984
22	95.454	106.237	56.713	9.947
23	95.215	111.159	55.866	9.852
24	94.726	115.948	54.514	9.612
25	94.792	120.760	53.159	9.566

Table D.2 Course B

Target	x	y	z	Best δt
1	75	5	50	N/A
2	75.514	9.942	50.561	9.884
3	76.280	14.801	51.459	9.825
4	76.464	19.731	52.270	9.800
5	76.788	24.651	53.100	9.857
6	77.619	29.517	53.893	9.822
7	78.714	34.369	54.406	9.933
8	80.191	39.111	54.981	9.903
9	82.247	43.558	55.978	9.723
10	83.945	48.008	57.501	9.500
11	85.987	52.139	59.440	9.186
12	88.368	56.088	61.373	9.196
13	90.182	60.266	63.436	9.039
14	91.667	64.362	65.889	9.812
15	92.799	68.246	68.827	11.755
16	93.692	72.084	71.905	12.311
17	94.672	75.833	75.064	12.636
18	96.247	79.760	77.729	10.659
19	97.585	83.600	80.639	11.639
20	98.424	87.377	83.806	12.669
21	99.684	90.714	87.309	14.012
22	101.492	93.759	90.839	14.118
23	102.575	96.682	94.748	15.637
24	103.974	99.466	98.659	15.643
25	105.626	101.705	102.813	16.618

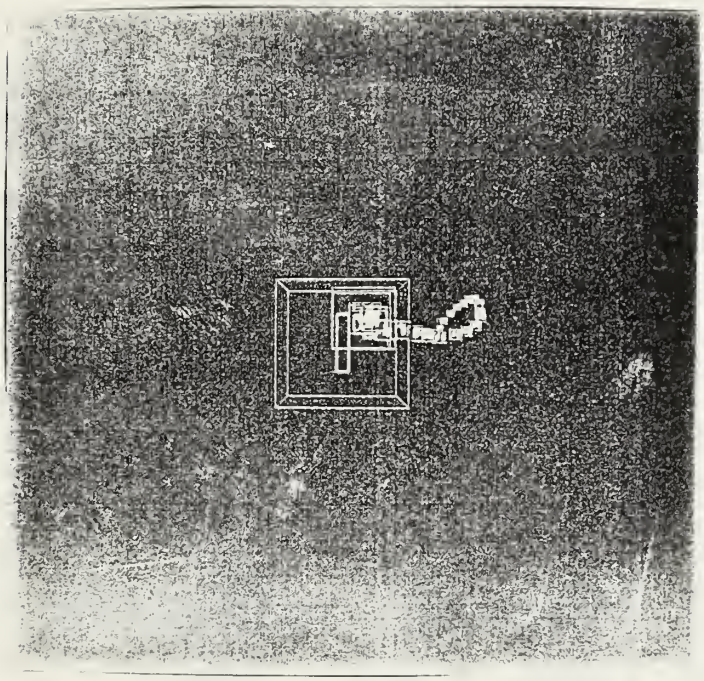

Figure D.1 Course A (operator's display with 60° FOV)

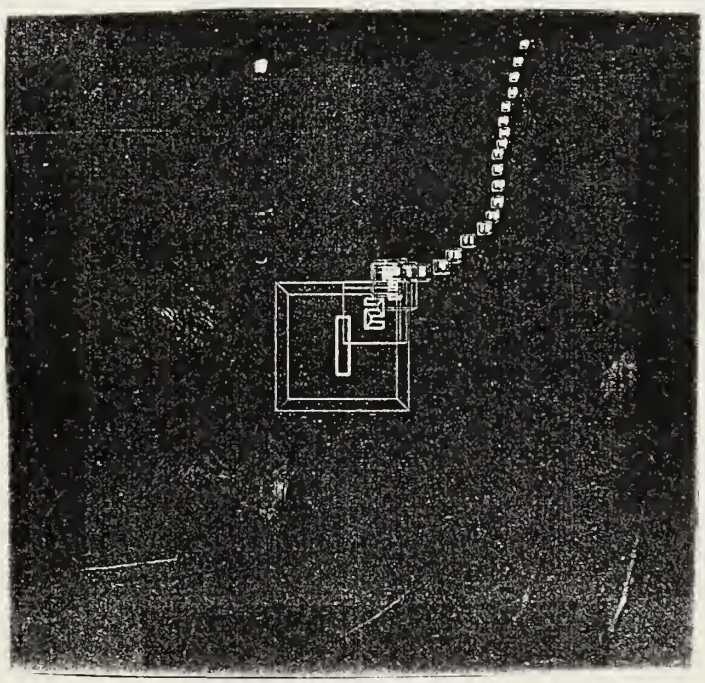

Figure D.2 Course B (operator's display with 60° FOV)

Table D.3 Course C

Target	x	y	z	Best δt
1	75	5	50	N/A
2	75.020	9.983	50.415	9.965
3	74.980	14.977	50.180	9.988
4	74.925	19.976	50.095	9.999
5	75.269	24.919	49.429	9.879
6	75.592	29.763	48.232	9.709
7	76.443	34.610	47.343	9.786
8	77.675	39.396	46.586	9.855
9	78.482	44.192	45.423	9.690
10	79.342	48.955	44.170	9.680
11	80.071	53.561	42.368	9.325
12	80.670	58.230	40.681	9.410
13	81.492	63.000	39.427	9.672
14	82.575	67.842	38.810	9.911
15	83.997	72.636	38.769	9.974
16	85.192	77.489	38.898	9.986
17	86.296	82.364	39.015	9.995
18	87.120	87.270	38.511	9.932
19	88.257	92.015	37.420	9.738
20	89.117	96.742	36.035	9.594
21	89.412	101.410	34.268	9.297
22	89.760	106.245	33.043	9.695
23	89.707	111.017	31.552	9.516
24	89.728	115.746	29.930	9.458
25	89.851	120.359	28.004	9.226

Table D.4 Course D

Target	x	y	z	Best δt
1	75	5	50	N/A
2	74.372	9.917	50.658	9.835
3	74.614	14.903	50.928	9.835
4	74.826	19.671	52.420	9.544
5	75.283	24.294	54.270	9.278
6	76.893	28.957	55.080	9.601
7	79.632	33.111	55.573	9.637
8	82.281	37.123	56.946	9.615
9	85.192	41.067	57.934	9.787
10	87.250	45.189	59.876	9.073
11	89.045	48.851	62.768	11.570
12	91.190	52.496	65.436	10.670
13	93.106	56.769	67.187	9.327
14	94.735	61.062	69.167	9.169
15	95.491	65.646	71.015	9.134
16	95.769	70.151	73.167	8.993
17	95.051	74.059	76.202	12.139
18	94.195	78.131	78.975	11.092
19	94.587	82.593	81.196	8.885
20	95.963	86.945	83.236	8.962
21	96.694	91.569	84.993	9.265
22	98.573	96.153	85.668	9.709
23	100.225	100.734	86.802	9.734
24	101.228	105.627	86.583	9.845
25	101.964	110.571	86.428	9.981

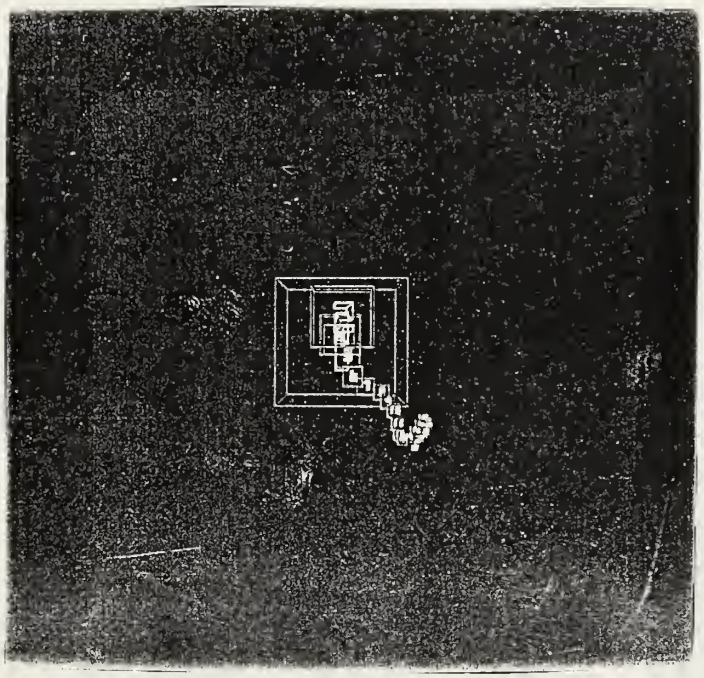

Figure D.3 Course C (operator's display with 60° FOV)

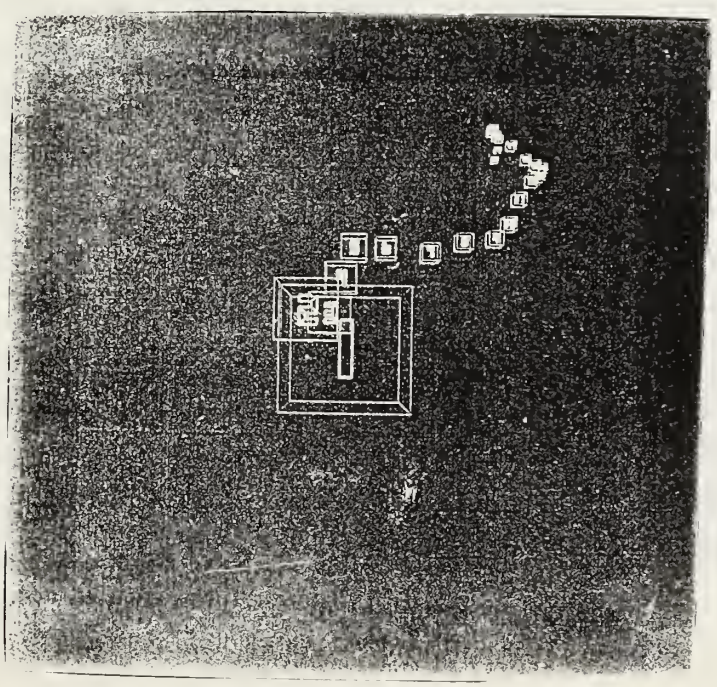

Figure D.4 Course D (operator's display with 60° FOV)

Table D.5 Course E

Target	x	y	z	Best δt
1	75	5	50	N/A
2	74.164	9.874	50.737	9.752
3	72.990	14.566	52.005	9.649
4	72.104	19.139	53.823	9.301
5	70.407	23.580	55.370	9.378
6	68.214	28.060	55.718	9.917
7	66.758	32.567	57.322	9.357
8	64.791	36.764	59.197	9.209
9	63.625	41.499	60.302	9.599
10	61.257	45.902	60.362	9.663
11	59.506	50.584	60.486	9.905
12	58.125	55.374	60.874	9.939
13	57.941	60.311	61.644	9.591
14	58.232	65.298	61.853	9.945
15	59.369	70.150	62.256	9.822
16	60.703	74.966	62.424	9.986
17	63.211	79.278	62.770	9.653
18	65.725	83.598	62.902	9.997
19	68.894	87.449	63.255	9.849
20	71.096	91.933	63.470	9.728
21	73.080	96.326	64.797	9.633
22	75.684	100.527	65.557	9.796
23	77.857	105.028	65.683	9.949
24	79.568	109.626	64.715	9.780
25	81.847	113.963	63.718	9.723

Table D.6 Course F

Target	x	y	z	Best δt
1	75	5	50	N/A
2	74.090	9.822	50.957	9.651
3	72.789	14.460	52.299	9.602
4	71.500	18.826	54.367	9.105
5	71.318	23.509	56.109	9.130
6	71.669	28.250	57.657	9.453
7	70.716	32.909	59.205	9.185
8	69.282	37.669	59.737	9.897
9	67.473	42.322	60.019	9.952
10	65.537	46.929	60.170	9.991
11	63.072	51.277	60.311	9.927
12	61.000	55.811	59.923	9.936
13	58.565	60.063	58.930	9.756
14	56.794	64.739	58.944	9.864
15	53.946	68.755	58.072	9.523
16	51.351	73.023	57.847	9.966
17	49.014	77.376	57.080	9.867
18	45.742	80.745	55.364	9.074
19	41.720	83.431	54.096	9.457
20	38.238	87.010	53.838	9.831
21	34.887	90.688	54.334	9.950
22	31.512	94.286	53.521	9.864
23	29.020	98.614	53.754	9.792
24	27.165	103.247	54.071	9.886
25	25.496	107.871	53.158	9.806

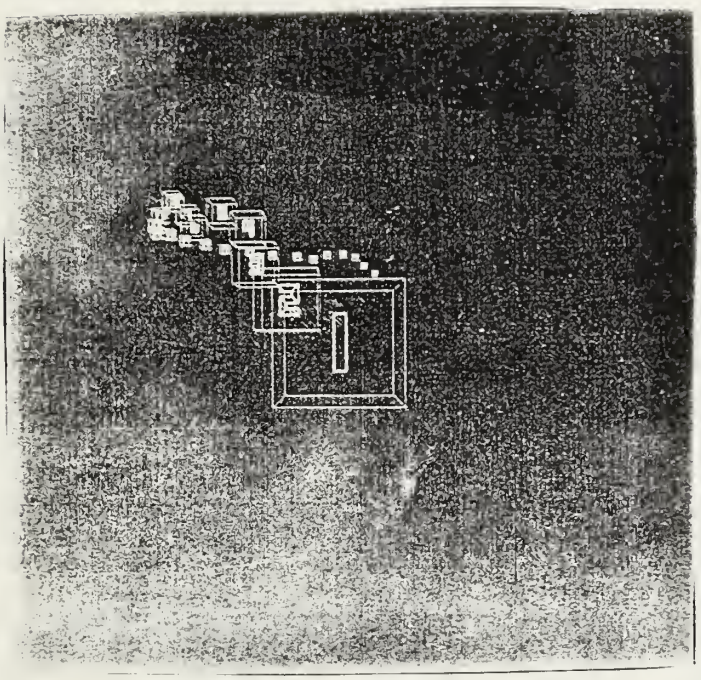

Figure D.5 Course E (operator's display with 60° FOV)

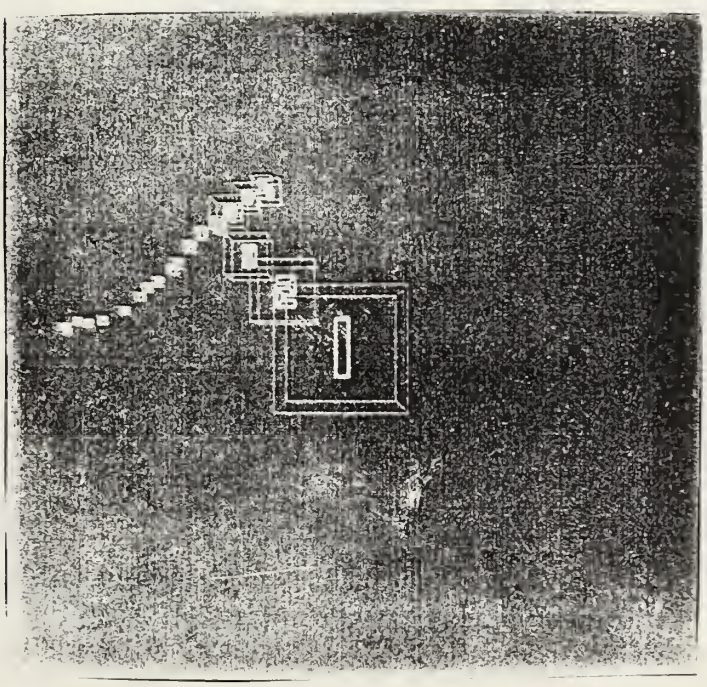

Figure D.6 Course F (operator's display with 60° FOV)

Table D.7 Course G

Target	x	y	z	Best δt
1	75	5	50	N/A
2	77.402	9.372	49.658	9.584
3	80.930	12.001	47.283	9.501
4	85.722	13.316	46.731	8.949
5	90.100	13.069	44.328	9.609
6	95.045	13.750	44.040	9.983
7	99.803	12.432	43.248	9.344
8	104.761	12.926	42.829	9.532
9	109.181	12.034	44.988	8.637
10	111.078	10.074	49.179	16.763
11	110.555	7.725	53.562	17.531
12	110.822	7.113	58.517	19.820
13	112.792	8.030	63.020	18.011
14	115.272	10.445	66.628	14.434
15	116.622	14.175	69.671	12.174
16	118.163	16.656	73.730	16.233
17	117.290	18.362	78.348	18.473
18	118.453	19.258	83.127	19.118
19	120.460	18.207	87.585	17.829
20	123.046	15.938	91.212	14.510
21	126.242	14.134	94.609	13.584
22	130.759	13.240	96.559	8.860
23	135.067	14.923	98.456	9.114
24	139.759	16.585	98.932	9.935
25	144.021	18.058	101.093	8.962

Table D.8 Course H

Target	x	y	z	Best δt
1	75	5	50	N/A
2	73.035	9.488	50.999	9.010
3	71.086	14.085	51.257	9.987
4	69.943	18.154	53.928	10.684
5	68.558	21.353	57.512	14.338
6	65.215	23.831	60.286	11.093
7	60.466	25.325	60.742	9.566
8	55.907	26.833	62.137	9.558
9	52.630	30.596	62.454	9.227
10	52.017	35.556	62.305	9.426
11	51.968	40.348	63.733	9.281
12	50.143	44.961	64.353	9.166
13	46.707	48.593	64.334	9.257
14	43.809	52.163	66.298	8.822
15	40.102	55.081	67.954	9.230
16	36.661	57.474	70.681	10.907
17	33.390	57.996	74.426	14.981
18	31.969	58.438	79.200	19.094
19	29.845	57.500	83.628	17.712
20	29.339	57.006	88.577	19.799
21	26.730	57.726	92.782	16.818
22	22.486	57.380	95.403	10.483
23	18.256	58.209	97.936	10.135
24	14.084	60.827	98.797	9.851
25	9.687	62.529	100.460	9.427

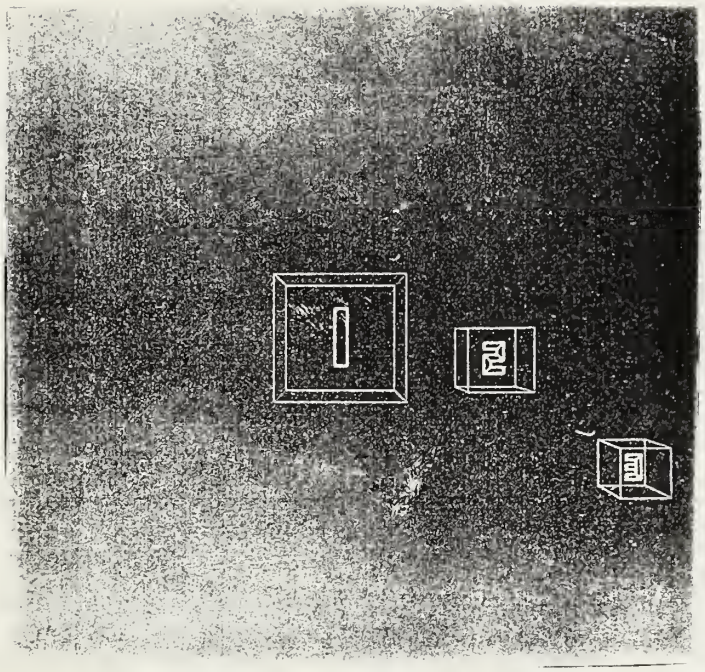

Figure D.7 Course G (operator's display with 60° FOV)

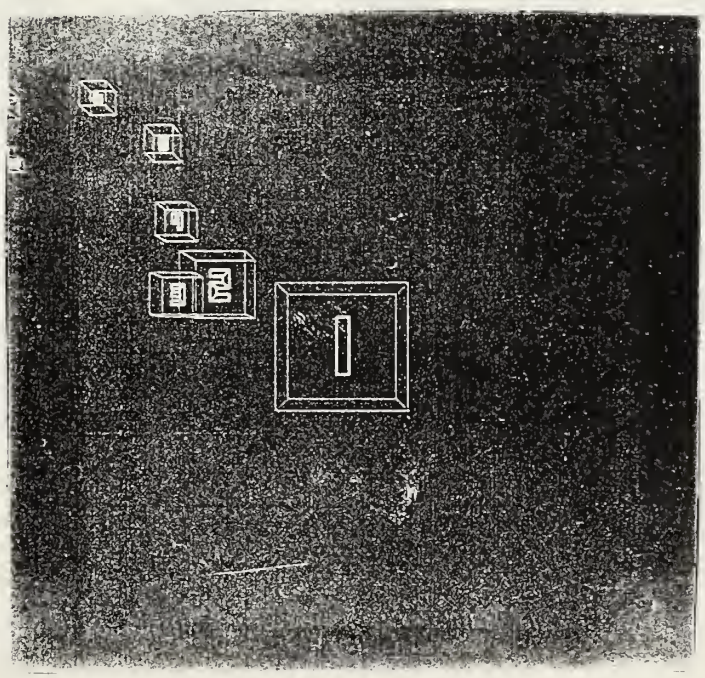

Figure D.8 Course H (operator's display with 60° FOV)

Table D.9 Course I

Target	x	y	z	Best δt
1	75	5	50	N/A
2	73.705	9.827	49.845	9.654
3	70.962	13.348	47.593	9.011
4	69.007	17.733	46.196	9.422
5	65.232	20.735	44.877	8.664
6	61.594	24.027	43.913	9.805
7	59.815	28.690	43.604	9.113
8	59.727	33.487	45.011	9.341
9	58.587	38.275	45.893	9.711
10	55.693	41.610	48.238	9.379
11	53.396	44.963	51.151	11.651
12	50.001	45.848	54.713	14.250
13	47.180	43.768	58.279	14.261
14	46.505	40.286	61.803	14.096
15	45.997	37.783	66.101	17.195
16	45.976	34.940	70.214	16.450
17	45.205	32.056	74.225	16.044
18	44.872	28.706	77.922	14.787
19	42.788	24.785	80.222	9.200
20	39.883	20.716	80.238	8.983
21	35.754	18.089	81.262	9.452
22	31.130	17.307	79.527	8.462
23	26.277	16.223	80.051	9.048
24	21.766	15.832	77.931	8.483
25	17.182	17.512	76.854	9.276

Table D.10 Course J

Target	x	y	z	Best δt
1	75	5	50	N/A
2	74.660	9.971	50.419	9.942
3	74.317	14.959	50.393	10.000
4	74.257	19.937	50.862	9.940
5	73.663	24.897	51.060	9.935
6	72.796	29.809	50.703	9.959
7	71.599	34.662	50.821	9.975
8	70.152	39.447	50.718	9.984
9	69.008	44.314	50.665	9.980
10	67.879	49.184	50.707	10.000
11	66.190	53.888	50.570	9.928
12	63.923	58.330	50.930	9.894
13	61.906	62.885	51.366	9.947
14	59.907	67.411	52.085	9.896
15	58.334	72.019	53.219	9.704
16	57.239	76.807	54.158	9.770
17	56.324	81.488	55.659	9.536
18	55.924	86.374	56.640	9.742
19	55.050	91.283	57.016	9.935
20	54.653	96.261	57.262	9.940
21	54.405	101.250	57.047	9.984
22	54.546	106.237	56.713	9.947
23	54.785	111.159	55.866	9.852
24	55.274	115.948	54.514	9.612
25	55.208	120.760	53.159	9.566

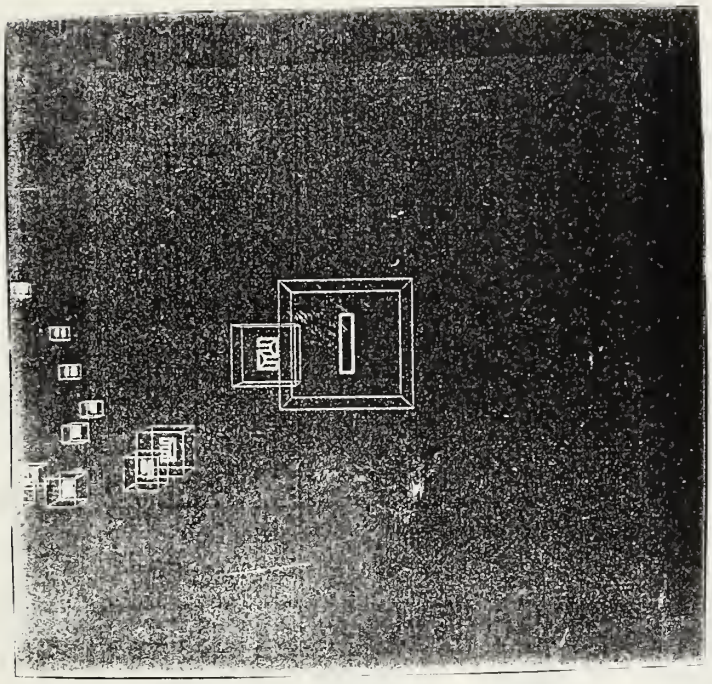

Figure D.9 Course I (operator's display with 60° FOV)

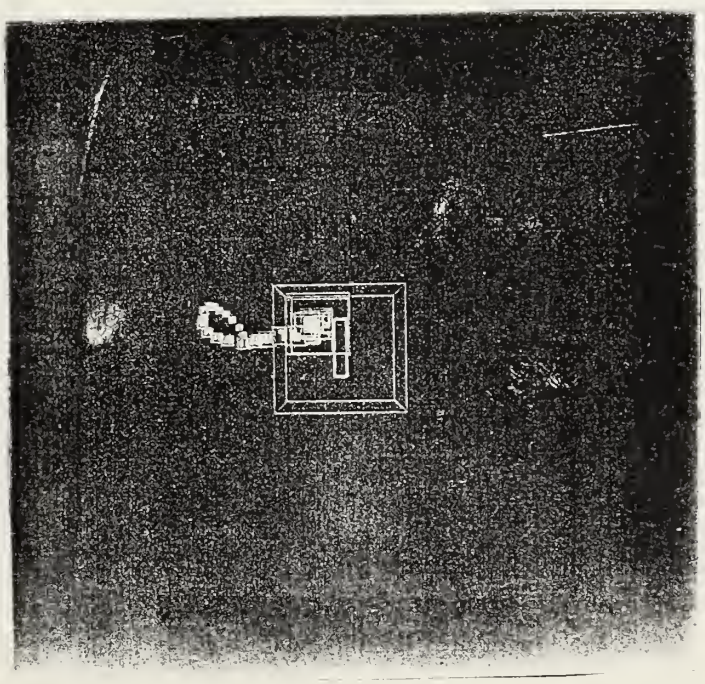

Figure D.10 Course J (operator's display with 60° FOV)

Table D.11 Course K

Target	x	y	z	Best δt
1	75	5	50	N/A
2	74.486	9.942	50.561	9.884
3	73.720	14.801	51.459	9.825
4	73.536	19.731	52.270	9.800
5	73.212	24.651	53.100	9.857
6	72.381	29.517	53.893	9.822
7	71.286	34.369	54.406	9.933
8	69.809	39.111	54.981	9.903
9	67.753	43.558	55.978	9.723
10	66.055	48.008	57.501	9.500
11	64.013	52.139	59.440	9.186
12	61.632	56.088	61.373	9.196
13	59.818	60.266	63.436	9.039
14	58.333	64.362	65.889	9.812
15	57.201	68.246	68.827	11.755
16	56.308	72.084	71.905	12.311
17	55.328	75.833	75.064	12.636
18	53.753	79.760	77.729	10.659
19	52.415	83.600	80.639	11.639
20	51.576	87.377	83.806	12.669
21	50.316	90.714	87.309	14.012
22	48.508	93.759	90.839	14.118
23	47.425	96.682	94.748	15.637
24	46.026	99.466	98.659	15.643
25	44.374	101.705	102.813	16.618

Table D.12 Course L

Target	x	y	z	Best δt
1	75	5	50	N/A
2	74.980	9.983	50.415	9.965
3	75.020	14.977	50.180	9.988
4	75.075	19.976	50.095	9.999
5	74.731	24.919	49.429	9.879
6	74.408	29.763	48.232	9.709
7	73.557	34.610	47.343	9.786
8	72.325	39.396	46.586	9.855
9	71.518	44.192	45.423	9.690
10	70.658	48.955	44.170	9.680
11	69.929	53.561	42.368	9.325
12	69.330	58.230	40.681	9.410
13	68.508	63.000	39.427	9.672
14	67.425	67.842	38.810	9.911
15	66.003	72.636	38.769	9.974
16	64.808	77.489	38.898	9.986
17	63.704	82.364	39.015	9.995
18	62.880	87.270	38.511	9.932
19	61.743	92.015	37.420	9.738
20	60.883	96.742	36.035	9.594
21	60.588	101.410	34.268	9.297
22	60.240	106.245	33.043	9.695
23	60.293	111.017	31.552	9.516
24	60.272	115.746	29.930	9.458
25	60.149	120.359	28.004	9.226

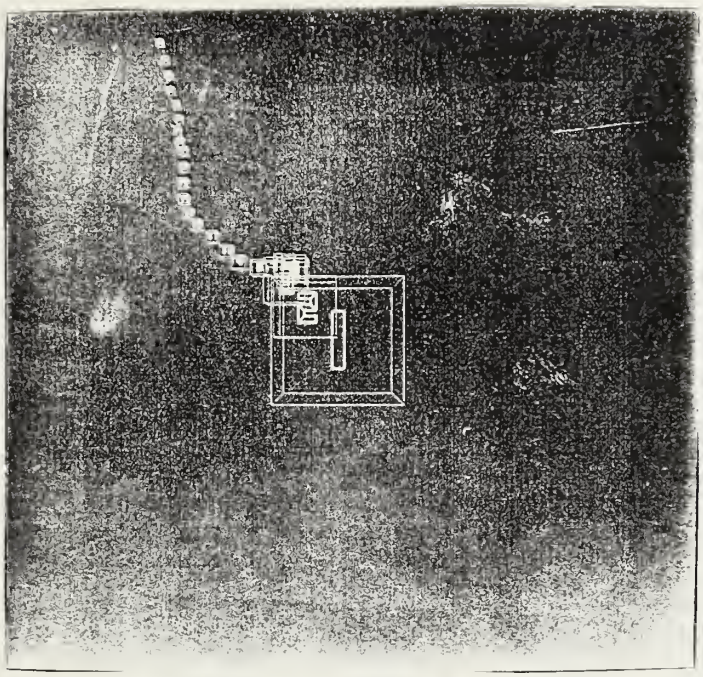

Figure D.11 Course K (operator's display with 60° FOV)

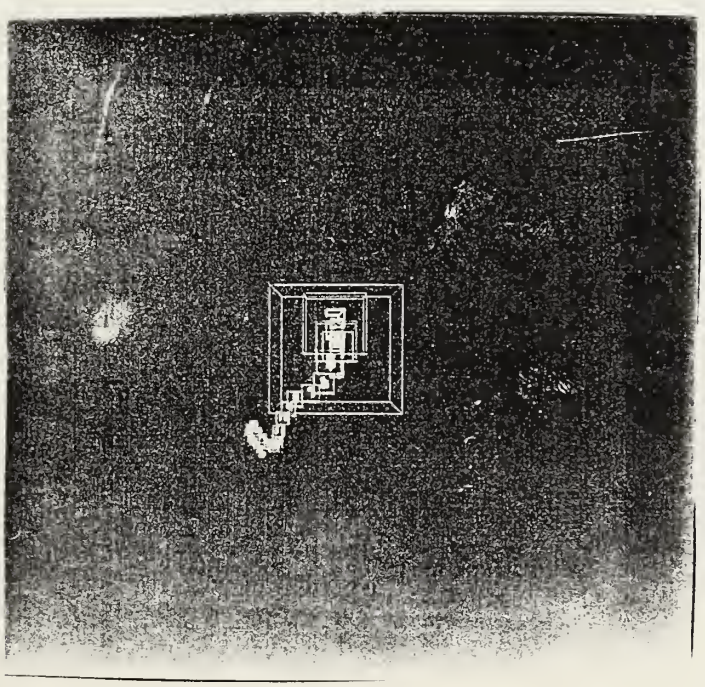

Figure D.12 Course L (operator's display with 60° FOV)

Table D.13 Course M

Target	x	y	z	Best δt
1	75	5	50	N/A
2	75.628	9.917	50.658	9.835
3	75.386	14.903	50.928	9.835
4	75.174	19.671	52.420	9.544
5	74.717	24.294	54.270	9.278
6	73.107	28.957	55.080	9.601
7	70.368	33.111	55.573	9.637
8	67.719	37.123	56.946	9.615
9	64.808	41.067	57.934	9.787
10	62.750	45.189	59.876	9.073
11	60.955	48.851	62.768	11.570
12	58.810	52.496	65.436	10.670
13	56.894	56.769	67.187	9.327
14	55.265	61.062	69.167	9.169
15	54.509	65.646	71.015	9.134
16	54.231	70.151	73.167	8.993
17	54.949	74.059	76.202	12.139
18	55.805	78.131	78.975	11.092
19	55.413	82.593	81.196	8.885
20	54.037	86.945	83.236	8.962
21	53.306	91.569	84.993	9.265
22	51.427	96.153	85.668	9.709
23	49.775	100.734	86.802	9.734
24	48.772	105.627	86.583	9.845
25	48.036	110.571	86.428	9.981

Table D.14 Course N

Target	x	y	z	Best δt
1	75	5	50	N/A
2	75.836	9.874	50.737	9.752
3	77.010	14.566	52.005	9.649
4	77.896	19.139	53.823	9.301
5	79.593	23.580	55.370	9.378
6	81.786	28.060	55.718	9.917
7	83.242	32.567	57.322	9.357
8	85.209	36.764	59.197	9.209
9	86.375	41.499	60.302	9.599
10	88.743	45.902	60.362	9.663
11	90.494	50.584	60.486	9.905
12	91.875	55.374	60.874	9.939
13	92.059	60.311	61.644	9.591
14	91.768	65.298	61.853	9.945
15	90.631	70.150	62.256	9.822
16	89.297	74.966	62.424	9.986
17	86.789	79.278	62.770	9.653
18	84.275	83.598	62.902	9.997
19	81.106	87.449	63.255	9.849
20	78.904	91.933	63.470	9.728
21	76.920	96.326	64.797	9.633
22	74.316	100.527	65.557	9.796
23	72.143	105.028	65.683	9.949
24	70.432	109.626	64.715	9.780
25	68.153	113.963	63.718	9.723

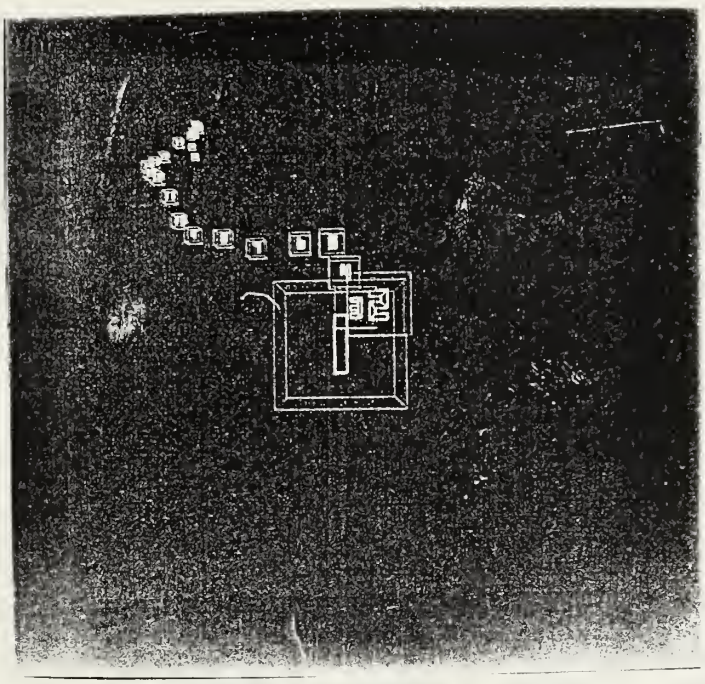

Figure D.13 Course M (operator's display with 60° FOV)

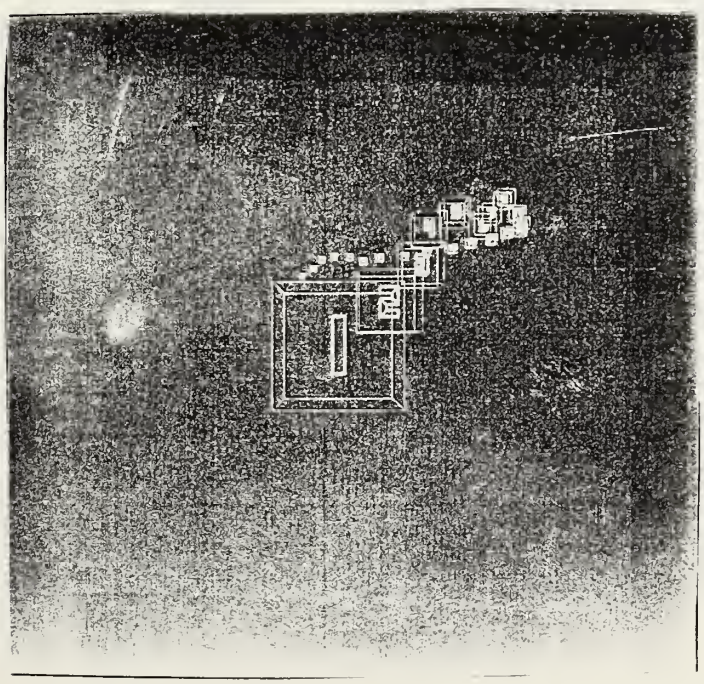

Figure D.14 Course N (operator's display with 60° FOV)

Table D.15 Course O

Target	x	y	z	Best δt
1	75	5	50	N/A
2	75.910	9.822	50.957	9.651
3	77.211	14.460	52.299	9.602
4	78.500	18.826	54.367	9.105
5	78.682	23.509	56.109	9.130
6	78.331	28.250	57.657	9.453
7	79.284	32.909	59.205	9.185
8	80.718	37.669	59.737	9.897
9	82.527	42.322	60.019	9.952
10	84.463	46.929	60.170	9.991
11	86.928	51.277	60.311	9.927
12	89.000	55.811	59.923	9.936
13	91.435	60.063	58.930	9.756
14	93.206	64.739	58.944	9.864
15	96.054	68.755	58.072	9.523
16	98.649	73.023	57.847	9.966
17	100.986	77.376	57.080	9.867
18	104.258	80.745	55.364	9.074
19	108.280	83.431	54.096	9.457
20	111.762	87.010	53.838	9.831
21	115.113	90.688	54.334	9.950
22	118.488	94.286	53.521	9.864
23	120.980	98.614	53.754	9.792
24	122.835	103.247	54.071	9.886
25	124.504	107.871	53.158	9.806

Table D.16 Course P

Target	x	y	z	Best δt
1	75	5	50	N/A
2	72.598	9.372	49.658	9.584
3	69.070	12.001	47.283	9.501
4	64.278	13.316	46.731	8.949
5	59.900	13.069	44.328	9.609
6	54.955	13.750	44.040	9.983
7	50.197	12.432	43.248	9.344
8	45.239	12.926	42.829	9.532
9	40.819	12.034	44.988	8.637
10	38.922	10.074	49.179	16.763
11	39.445	7.725	53.562	17.531
12	39.178	7.113	58.517	19.820
13	37.208	8.030	63.020	18.011
14	34.728	10.445	66.628	14.434
15	33.378	14.175	69.671	12.174
16	31.837	16.656	73.730	16.233
17	32.710	18.362	78.348	18.473
18	31.547	19.258	83.127	19.118
19	29.540	18.207	87.585	17.829
20	26.954	15.938	91.212	14.510
21	23.758	14.134	94.609	13.584
22	19.241	13.240	96.559	8.860
23	14.933	14.923	98.456	9.114
24	10.241	16.585	98.932	9.935
25	5.979	18.058	101.093	8.962

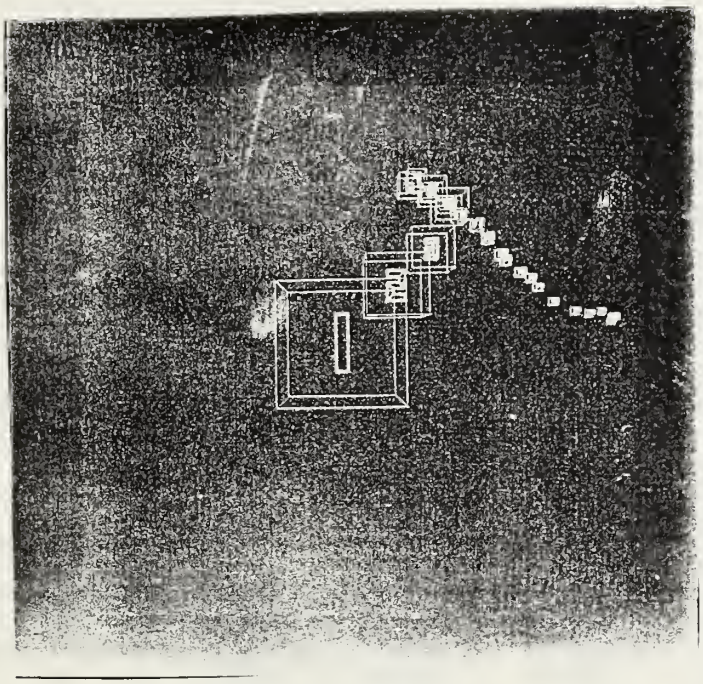

Figure D.15 Course O (operator's display with 60° FOV)

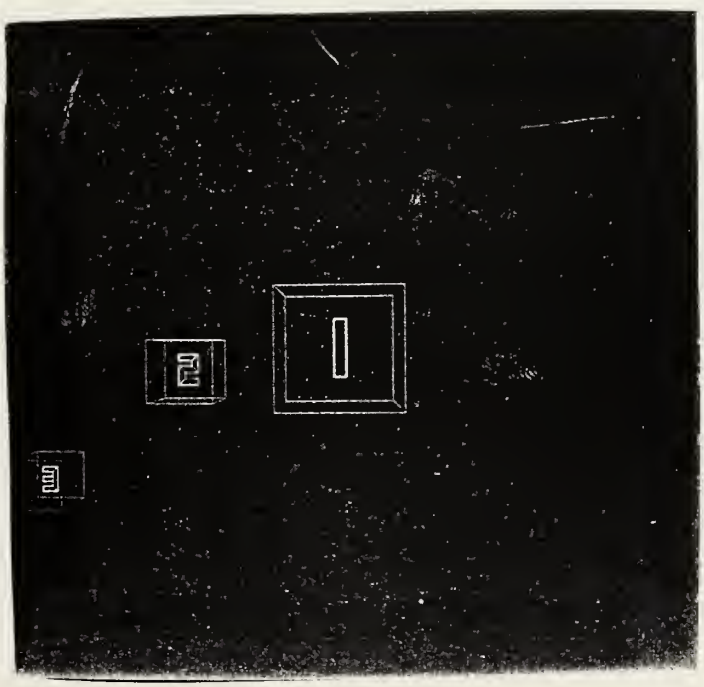

Figure D.16 Course P (operator's display with 60° FOV)

Table D.17 Course Q

Target	x	y	z	Best δt
1	75	5	50	N/A
2	76.965	9.488	50.999	9.010
3	78.914	14.085	51.257	9.987
4	80.057	18.154	53.928	10.684
5	81.442	21.353	57.512	14.338
6	84.785	23.831	60.286	11.093
7	89.534	25.325	60.742	9.566
8	94.093	26.833	62.137	9.558
9	97.370	30.596	62.454	9.227
10	97.983	35.556	62.305	9.426
11	98.032	40.348	63.733	9.281
12	99.857	44.961	64.353	9.166
13	103.293	48.593	64.334	9.257
14	106.191	52.163	66.298	8.822
15	109.898	55.081	67.954	9.230
16	113.339	57.474	70.681	10.907
17	116.610	57.996	74.426	14.981
18	118.031	58.438	79.200	19.094
19	120.155	57.500	83.628	17.712
20	120.661	57.006	88.577	19.799
21	123.270	57.726	92.782	16.818
22	127.514	57.380	95.403	10.483
23	131.744	58.209	97.936	10.135
24	135.916	60.827	98.797	9.851
25	140.313	62.529	100.460	9.427

Table D.18 Course R

Target	x	y	z	Best δt
1	75	5	50	N/A
2	76.295	9.827	49.845	9.654
3	79.038	13.348	47.593	9.011
4	80.993	17.733	46.196	9.422
5	84.768	20.735	44.877	8.664
6	88.406	24.027	43.913	9.805
7	90.185	28.690	43.604	9.113
8	90.273	33.487	45.011	9.341
9	91.413	38.275	45.893	9.711
10	94.307	41.610	48.238	9.379
11	96.604	44.963	51.151	11.651
12	99.999	45.848	54.713	14.250
13	102.820	43.768	58.279	14.261
14	103.495	40.286	61.803	14.096
15	104.003	37.783	66.101	17.195
16	104.024	34.940	70.214	16.450
17	104.795	32.056	74.225	16.044
18	105.128	28.706	77.922	14.787
19	107.212	24.785	80.222	9.200
20	110.117	20.716	80.238	8.983
21	114.246	18.089	81.262	9.452
22	118.870	17.307	79.527	8.462
23	123.723	16.223	80.051	9.048
24	128.234	15.832	77.931	8.483
25	132.818	17.512	76.854	9.276

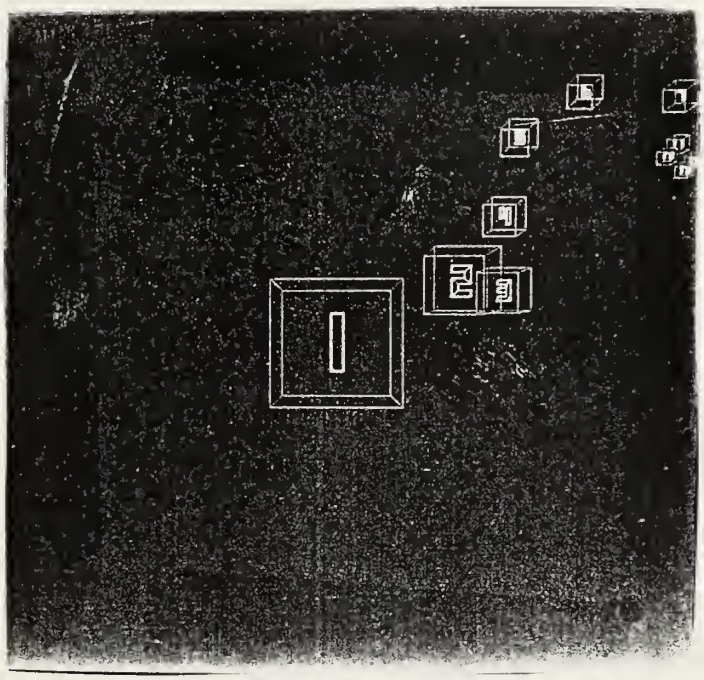

Figure D.17 Course Q (operator's display with 60° FOV)

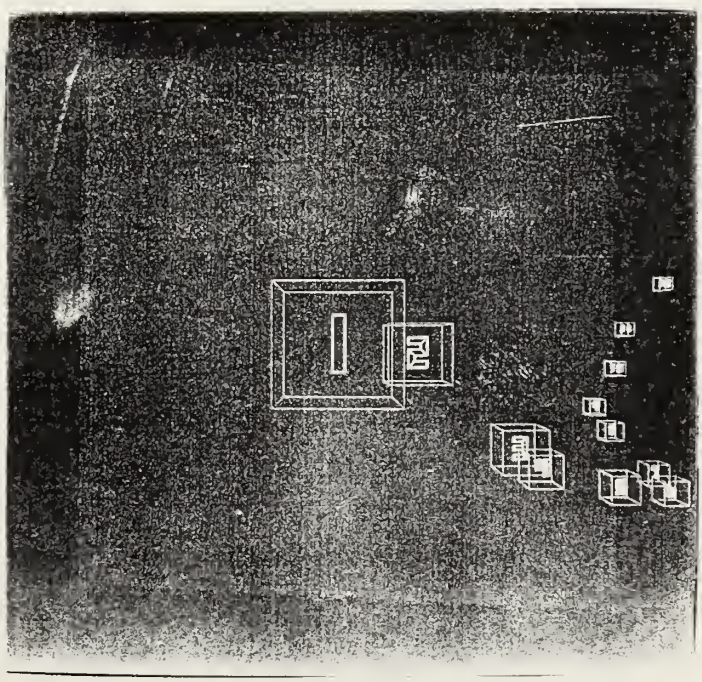

Figure D.18 Course R (operator's display with 60° FOV)

Table D.19 Course X

Target	x	y	z
1	75	5	50
2	75.415	9.975	50.274
3	75.804	14.960	50.278
4	76.682	19.878	50.081
5	77.443	24.817	49.909
6	78.169	29.761	50.092
7	79.052	34.674	49.800
8	80.541	39.441	50.037
9	81.479	44.352	50.041
10	82.073	49.286	50.595
11	82.721	54.141	51.598
12	83.762	58.762	53.199
13	85.367	62.995	55.321
14	87.501	66.919	57.568
15	89.307	71.089	59.653
16	91.327	75.215	61.627
17	93.395	79.426	63.357
18	95.436	83.409	65.587
19	98.061	87.359	67.170
20	100.328	91.501	68.815
21	102.772	95.558	70.417
22	105.399	99.343	72.359
23	107.766	103.514	73.773
24	109.633	107.777	75.602
25	111.801	111.855	77.516

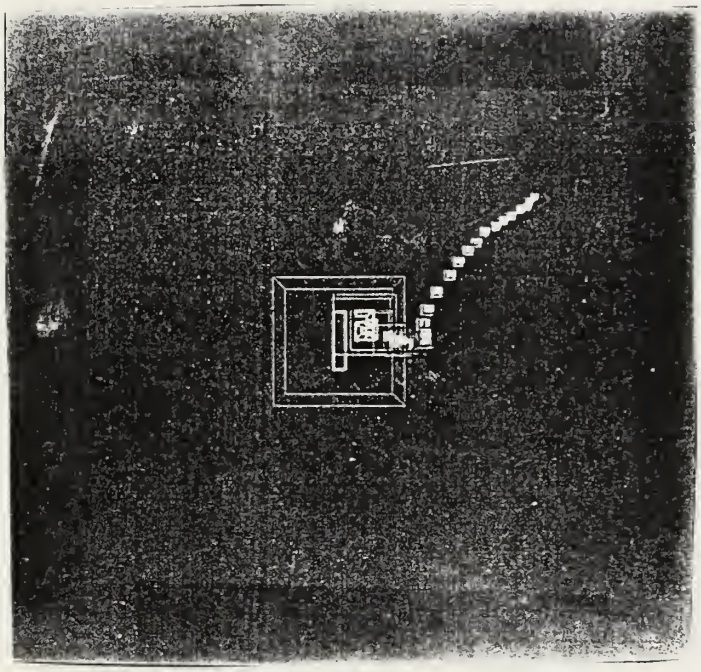

Figure D.19 Course X (operator's display with 60° FOV)

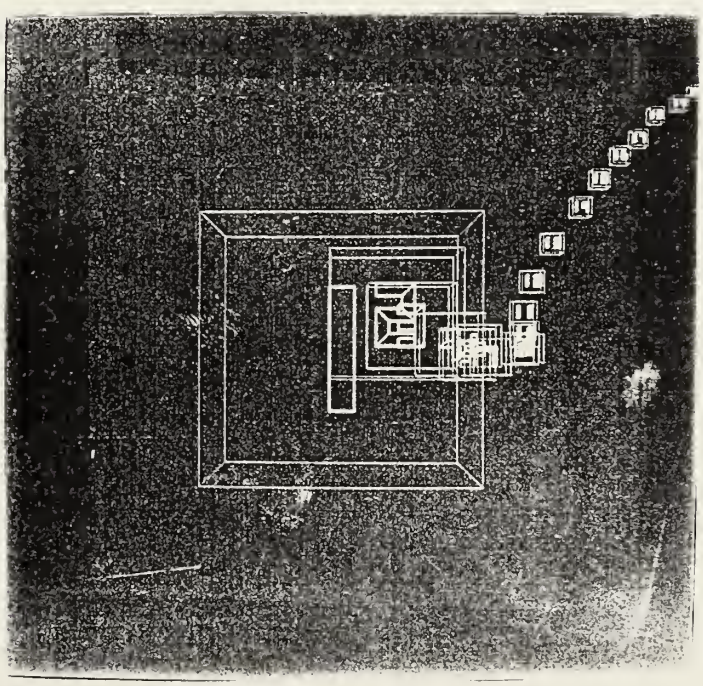

Figure D.20 Course X (operator's display with 30° FOV)

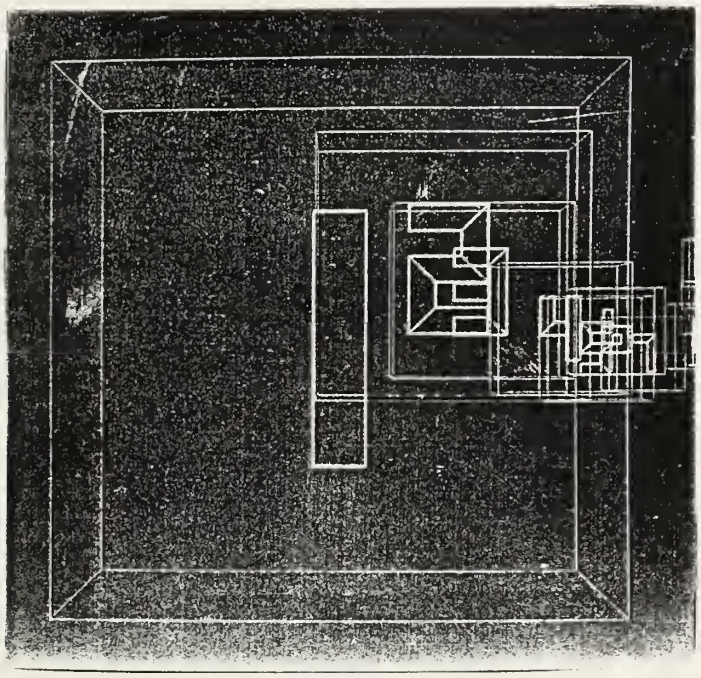

Figure D.21 Course X (operator's display with 15° FOV)

APPENDIX E

Raw Data

Tables E.1 through E.12 list the data for each of the four operators over all seven tests. The tabulated values are the time differences between successive targets in seconds. Value 1 is the time difference between hitting targets 1 and 2, value 2 for targets 2 and 3, etc. The total for each column is indicated at the bottom of the column. For all tests the course letter is specified at the top of its respective column. For Test 1 the operator's field of view is also shown.

Table E.1 Operator I, Test 1

	60° FOV			30° FOV			15° FOV		
	A	D	G	B	E	H	C	F	I
1	16	16	13	55	53	35	12	53	42
2	10	17	39	50	59	38	39	90	49
3	14	15	16	33	67	101	28	74	29
4	15	37	28	40	78	59	33	31	45
5	15	22	32	36	79	48	35	82	79
6	15	22	22	33	55	34	75	50	43
7	14	15	14	33	27	23	72	96	32
8	11	17	28	194	25	39	83	60	33
9	11	27	129	48	11	11	76	21	219
10	11	35	88	64	32	36	92	33	27
11	18	29	180	31	82	22	89	43	189
12	17	24	67	116	37	41	51	31	221
13	15	18	34	75	14	106	63	19	46
14	14	20	18	39	68	44	69	61	47
15	46	19	25	73	69	94	32	26	59
16	36	49	44	77	157	52	43	93	109
17	16	21	78	50	38	195	56	33	114
18	15	31	93	24	14	48	42	22	25
19	13	18	104	51	21	46	89	25	41
20	12	16	38	85	47	60	35	21	83
21	11	21	51	30	17	57	40	24	22
22	11	16	38	47	11	26	34	19	21
23	10	18	27	152	41	42	33	16	28
24	66	12	12	52	18	60	32	13	138
Total	432	535	1218	1488	1120	1317	1253	1036	1741

Table E.2 Operator I - Tests 2, 3, and 4

	Test 2			Test 3			Test 4		
	J	M	P	K	N	Q	A	E	I
1	16	16	41	15	13	20	18	19	16
2	16	11	36	14	17	17	13	24	26
3	11	15	21	10	15	20	11	16	18
4	17	29	28	14	22	28	14	23	28
5	24	46	19	18	18	36	15	13	36
6	19	12	26	16	55	91	32	16	13
7	29	17	14	38	22	27	16	25	19
8	13	16	53	18	13	31	11	12	47
9	14	22	37	14	15	17	10	20	16
10	24	37	93	15	12	50	11	17	17
11	28	18	105	13	13	16	15	13	53
12	24	21	65	11	10	23	18	11	144
13	12	25	88	13	12	40	24	20	19
14	13	23	27	13	11	21	11	19	29
15	18	26	52	47	16	22	12	11	33
16	25	38	47	16	12	48	12	15	49
17	18	34	47	22	18	30	13	13	28
18	27	17	69	16	18	69	13	12	20
19	22	26	102	18	14	70	14	14	22
20	42	20	32	25	15	36	11	15	30
21	19	20	19	20	11	37	14	10	17
22	25	22	32	39	9	32	16	12	10
23	18	12	25	22	16	12	12	21	14
24	18	10	30	23	10	14	11	16	23
Total	492	533	1108	470	387	807	347	387	727

Table E.3 Operator I - Tests 5, 6, and 7

	Test 5			Test 6			Test 7		
	B	F	G	L	O	R	C	D	H
1	11	12	50	10	17	29	10	25	56
2	48	19	39	10	11	31	10	22	20
3	18	17	14	11	32	24	10	16	22
4	15	13	25	9	15	23	18	29	38
5	14	13	25	12	12	18	19	31	47
6	17	16	20	12	21	67	22	28	13
7	17	16	17	12	14	25	19	35	18
8	10	10	20	13	14	30	21	29	47
9	10	10	67	22	14	24	24	27	15
10	28	19	62	18	17	22	48	26	18
11	39	18	38	18	18	32	19	37	37
12	29	14	49	20	16	85	20	27	17
13	29	18	91	15	16	50	18	36	37
14	23	15	39	12	33	25	12	27	34
15	22	10	33	13	21	30	10	20	22
16	23	31	31	12	13	25	10	24	55
17	27	13	41	13	33	24	14	37	37
18	22	26	86	23	21	32	51	18	60
19	26	13	45	14	14	17	28	32	54
20	21	22	28	11	14	44	16	24	25
21	26	21	16	11	18	19	15	33	27
22	55	14	20	10	23	17	16	15	42
23	28	12	18	11	13	17	17	10	20
24	24	10	14	15	10	16	15	11	32
Total	582	382	888	327	430	726	462	619	793

Table E.4 Operator II - Test 1

	60° FOV			30° FOV			15° FOV		
	J	M	P	K	N	Q	L	O	R
1	14	15	18	22	39	40	27	32	25
2	15	32	88	15	31	49	22	44	68
3	12	44	13	43	76	38	51	28	61
4	10	18	53	20	45	38	16	31	26
5	12	57	12	25	32	203	33	38	41
6	10	35	97	15	53	52	67	124	19
7	36	23	20	76	29	35	71	29	47
8	66	21	75	15	30	52	78	92	88
9	19	15	239	24	36	74	32	37	43
10	23	107	77	16	33	23	32	115	77
11	19	47	51	116	62	16	34	48	87
12	24	44	69	37	24	93	36	80	115
13	31	20	55	30	26	185	25	59	98
14	63	30	54	59	77	27	41	99	94
15	19	21	56	30	13	43	36	44	86
16	25	27	38	110	49	32	20	59	47
17	14	20	259	87	16	63	69	245	347
18	82	20	132	31	20	59	17	56	130
19	42	16	87	61	24	43	34	130	220
20	27	13	66	44	35	63	34	263	133
21	11	12	85	60	43	57	274	43	113
22	19	27	34	52	63	30	31	57	97
23	29	19	51	42	17	29	85	71	160
24	87	10	34	70	86	19	125	72	61
Total	709	693	1763	1100	959	1363	1290	1896	2283

Table E.5 Operator II - Tests 2, 3, and 4

	Test 2			Test 3			Test 4		
	A	D	G	B	E	H	J	N	R
1	20	16	21	12	25	30	12	20	30
2	12	12	28	22	25	17	12	13	30
3	14	19	23	14	50	17	10	14	32
4	13	55	26	14	36	30	15	22	40
5	25	34	21	16	23	43	14	16	18
6	20	22	26	22	16	82	12	23	18
7	21	25	17	22	22	39	11	23	11
8	14	18	17	33	23	59	10	17	15
9	16	25	213	32	24	17	11	17	37
10	19	33	45	33	13	23	10	19	34
11	22	35	82	28	18	18	10	16	72
12	26	22	150	54	15	17	13	12	56
13	20	125	53	35	15	41	18	10	30
14	25	32	76	33	80	22	15	12	71
15	20	21	45	30	31	27	14	17	79
16	17	27	28	38	31	48	17	46	30
17	13	23	78	36	30	44	17	16	35
18	15	32	49	33	30	54	17	22	23
19	10	25	99	25	40	66	18	12	16
20	10	20	29	32	28	64	18	15	24
21	11	17	51	58	45	74	20	14	33
22	18	22	60	30	49	65	25	14	20
23	17	16	54	32	26	15	27	9	23
24	35	24	39	28	36	48	17	15	48
Total	433	700	1330	712	731	960	363	414	825

Table E.6 Operator II - Tests 5, 6, and 7

	Test 5			Test 6			Test 7		
	K	O	P	C	F	I	L	M	Q
1	11	22	50	13	12	31	20	25	19
2	10	20	37	27	14	48	17	20	28
3	12	25	25	30	21	26	17	24	41
4	13	23	25	21	10	32	53	20	40
5	11	22	25	17	26	28	28	21	50
6	12	22	13	27	20	22	20	58	38
7	10	21	14	17	14	17	23	26	28
8	11	25	18	16	13	20	45	28	21
9	16	15	37	25	19	22	33	22	27
10	18	13	52	22	19	23	37	23	22
11	18	14	54	19	18	74	19	23	37
12	21	43	32	19	22	136	32	23	14
13	25	25	39	16	12	72	22	25	27
14	26	18	43	23	18	87	14	23	28
15	29	15	36	27	17	23	26	26	53
16	30	20	42	16	13	40	53	38	76
17	20	23	35	16	25	41	25	37	181
18	19	28	54	16	21	38	24	32	50
19	25	33	32	13	12	22	23	20	46
20	21	19	28	15	19	28	22	19	41
21	30	14	49	17	21	45	26	17	37
22	80	11	42	16	11	94	16	20	44
23	37	12	19	19	16	32	19	27	42
24	31	12	28	19	38	51	38	12	16
Total	536	495	829	466	431	1052	652	609	1006

Table E.7 Operator III - Test 1

	60° FOV			30° FOV			15° FOV		
	B	E	H	C	F	I	A	D	G
1	10	29	21	10	54	31	14	10	222
2	12	78	16	11	40	49	11	10	398
3	11	39	49	13	53	65	20	185	28
4	10	29	39	64	45	88	55	153	287
5	11	40	32	52	61	47	24	33	46
6	11	34	18	69	47	39	18	30	29
7	10	28	23	54	35	113	29	46	32
8	10	54	27	76	44	170	13	19	35
9	10	14	18	59	47	149	9	26	124
10	36	11	27	67	69	109	11	31	182
11	9	11	17	101	45	203	14	116	68
12	15	12	10	70	50	95	17	28	82
13	14	110	19	76	86	61	53	24	101
14	16	33	34	63	99	90	24	20	71
15	68	17	20	48	47	93	28	21	42
16	57	12	76	57	43	32	41	37	72
17	17	18	25	55	59	30	17	37	37
18	15	42	86	65	61	120	11	158	102
19	62	17	256	70	40	17	10	32	230
20	42	29	101	69	46	17	9	34	397
21	19	30	45	73	53	21	10	21	127
22	142	28	41	85	29	17	13	62	26
23	99	20	46	67	62	26	14	9	23
24	66	38	117	43	31	65	13	10	44
Total	772	773	1163	1417	1246	1747	478	1152	2805

Table E.8 Operator III - Tests 2, 3, and 4

	Test 2			Test 3			Test 4		
	K	N	Q	L	O	R	B	F	G
1	14	28	26	10	16	13	19	15	63
2	30	18	18	10	18	20	36	12	35
3	33	34	28	33	21	11	26	16	79
4	34	18	51	28	32	22	12	38	25
5	20	19	29	102	13	15	21	38	26
6	29	21	23	44	40	11	58	24	29
7	20	17	72	12	17	14	12	13	18
8	19	31	43	17	20	21	21	17	17
9	13	28	17	21	79	14	16	24	73
10	19	15	76	22	64	23	26	10	110
11	36	17	36	20	22	54	20	13	94
12	28	22	15	15	12	32	20	14	45
13	68	14	65	58	34	26	25	13	55
14	32	20	29	10	16	70	17	15	33
15	20	23	30	10	16	40	19	12	37
16	67	31	47	11	43	44	26	16	55
17	27	26	38	12	22	43	18	23	37
18	23	21	51	33	64	11	19	22	74
19	24	25	39	15	30	21	34	16	54
20	29	23	47	97	12	54	32	13	29
21	33	15	41	21	30	28	36	17	19
22	46	11	31	16	20	20	30	17	23
23	40	18	62	9	11	15	40	11	14
24	36	12	21	9	19	55	36	13	46
Total	740	507	935	635	671	677	619	422	1090

Table E.9 Operator III - Tests 5, 6, and 7

	Test 5			Test 6			Test 7		
	C	D	H	J	M	P	A	E	I
1	10	21	15	11	26	11	16	24	20
2	10	10	10	9	15	34	19	23	62
3	10	20	23	43	22	19	21	51	59
4	13	58	33	16	37	23	20	23	35
5	21	14	23	12	69	15	12	35	46
6	46	14	20	11	24	45	21	27	20
7	17	21	15	10	18	19	24	58	41
8	44	17	30	10	17	36	15	44	38
9	41	21	16	11	13	49	24	25	25
10	54	14	36	10	69	72	26	19	32
11	19	26	28	14	28	83	21	20	108
12	48	21	17	10	35	71	28	30	98
13	24	22	22	9	31	68	56	19	66
14	20	22	14	12	30	75	22	18	27
15	17	23	21	10	26	63	19	17	29
16	15	24	33	18	31	50	30	19	58
17	14	21	51	16	24	58	35	13	51
18	15	21	42	11	30	48	11	32	67
19	24	20	52	57	32	49	24	20	35
20	10	38	39	15	35	51	26	37	20
21	12	11	48	14	25	38	17	104	35
22	10	10	52	16	23	65	26	36	17
23	25	10	22	9	19	26	50	28	19
24	23	10	18	16	17	14	24	28	26
Total	542	489	680	370	696	1082	587	750	1034

Table E.10 Operator IV - Test 1

	60° FOV			30° FOV			15° FOV		
	K	N	Q	L	O	R	J	M	P
1	38	23	25	40	51	79	76	46	35
2	37	46	32	44	46	77	86	30	51
3	30	27	51	38	69	51	67	132	48
4	49	25	38	62	39	61	48	61	110
5	54	41	38	70	39	83	64	297	54
6	39	49	20	39	24	19	53	50	277
7	67	25	23	43	27	61	43	73	56
8	51	48	33	79	18	48	30	24	316
9	28	42	24	26	15	183	21	51	140
10	25	36	22	36	14	61	49	52	310
11	22	49	20	40	11	253	46	34	219
12	23	25	20	25	29	270	31	51	152
13	33	15	34	26	37	171	104	202	179
14	42	31	31	41	42	282	135	216	258
15	45	19	35	22	38	119	43	45	90
16	32	21	56	17	14	141	97	61	127
17	30	24	46	20	46	95	40	54	96
18	49	18	74	33	48	61	99	176	88
19	39	21	33	29	15	20	127	58	104
20	66	22	145	26	25	69	121	69	64
21	75	35	28	20	171	79	46	14	44
22	44	47	40	19	53	66	32	40	63
23	36	31	66	38	35	100	57	41	121
24	45	14	46	47	39	20	60	30	79
Total	999	734	980	880	945	2469	1575	1907	3081

Table E.11 Operator IV - Tests 2, 3, and 4

	Test 2			Test 3			Test 4		
	B	E	H	C	F	I	K	O	P
1	11	17	19	11	15	21	12	11	29
2	20	22	13	12	38	23	23	17	41
3	16	21	40	10	21	18	18	24	18
4	17	27	41	12	16	53	35	26	23
5	17	37	54	17	12	30	21	22	16
6	14	21	21	15	16	22	16	17	15
7	13	17	28	13	19	17	17	13	18
8	22	22	19	22	19	14	11	30	22
9	20	19	19	18	18	22	11	18	46
10	35	22	16	55	16	24	13	10	56
11	36	26	16	19	18	109	15	43	25
12	18	13	58	17	31	77	16	16	152
13	14	10	20	14	16	77	14	14	48
14	17	16	23	11	21	109	14	17	22
15	15	12	32	13	36	29	18	18	35
16	17	16	60	14	27	36	23	13	103
17	53	12	59	12	16	26	19	16	76
18	18	20	66	14	11	23	18	13	84
19	52	18	133	12	14	11	21	11	59
20	29	18	36	15	11	19	22	13	31
21	28	20	42	11	11	20	67	14	16
22	68	17	31	12	18	17	29	14	37
23	22	11	22	10	15	13	53	10	11
24	17	11	17	9	10	17	43	10	28
Total	589	445	885	368	445	827	549	410	1011

Table E.12 Operator IV - Tests 5, 6, and 7

	Test 5			Test 6			Test 7		
	L	M	Q	A	D	G	J	N	R
1	11	17	17	19	15	25	12	32	12
2	12	11	11	29	17	23	14	34	35
3	10	17	20	20	13	19	23	28	71
4	14	13	24	13	60	28	17	24	24
5	13	11	21	12	30	16	13	23	18
6	12	11	16	13	12	15	13	22	40
7	19	13	58	16	13	18	14	24	25
8	13	11	16	13	14	24	14	25	29
9	12	12	15	22	19	45	15	14	28
10	17	17	38	20	29	84	12	20	23
11	13	20	14	10	20	43	21	16	60
12	14	17	15	11	19	61	26	19	61
13	39	13	17	10	25	58	28	12	53
14	11	22	19	12	22	99	25	20	172
15	10	18	124	11	13	51	20	14	42
16	10	19	32	10	75	40	35	23	44
17	52	17	75	11	29	92	24	17	31
18	14	27	91	9	21	72	13	18	22
19	12	14	45	11	26	73	13	19	11
20	12	16	52	20	20	23	25	17	26
21	15	9	35	17	20	16	32	23	26
22	12	10	25	13	17	22	18	13	19
23	10	10	14	10	12	15	14	20	24
24	9	10	23	48	11	28	26	14	18
Total	366	355	817	380	552	990	467	491	914

APPENDIX F

Normalized Data

Tables F.1 through F.12 list the data for each of the four operators over all seven tests. The tabulated values are normalized values from the associated tables in Appendix E. The data were normalized to remove effects properly attributed to variations in the level of course difficulty related to the Jason vehicle simulation model. The total, mean value, and standard deviation (σ) for each column are indicated at the bottom of the column. For all tests the course letter is specified at the top of its respective column. For Test 1 the operator's field of view is also shown.

The normalization procedure divided each time difference by the best time between the associated targets from Appendix D to arrive at the normalized value (dimensionless). Because the logged times represented the most recently passed whole second, while the best times between targets were calculated to a greater degree of precision, it was possible to achieve a normalized value of 0.9.

Table F.1 Operator I - Test 1

	60° FOV			30° FOV			15° FOV		
	A	D	G	B	E	H	C	F	I
1	1.6	1.6	1.4	5.6	5.4	3.9	1.2	5.5	4.4
2	1.0	1.7	4.1	5.1	6.1	3.8	3.9	9.4	5.4
3	1.4	1.6	1.8	3.4	7.2	9.5	2.8	8.1	3.1
4	1.5	4.0	2.9	4.1	8.3	4.1	3.3	3.4	5.2
5	1.5	2.3	3.2	3.7	8.0	4.3	3.6	8.7	8.1
6	1.5	2.3	2.4	3.3	5.9	3.6	7.7	5.4	4.7
7	1.4	1.6	1.5	3.3	2.9	2.4	7.3	9.7	3.4
8	1.1	1.7	3.2	20.0	2.6	4.2	8.6	6.0	3.4
9	1.1	3.0	7.7	5.1	1.1	1.2	7.9	2.1	23.4
10	1.1	3.0	5.0	7.0	3.2	3.9	9.9	3.3	2.3
11	1.8	2.7	9.1	3.4	8.3	2.4	9.5	4.3	13.3
12	1.7	2.6	3.7	12.8	3.9	4.4	5.3	3.2	15.5
13	1.5	2.0	2.4	7.6	1.4	12.0	6.4	1.9	3.3
14	1.4	2.2	1.5	3.3	6.9	4.8	6.9	6.4	2.7
15	4.7	2.1	1.5	5.9	6.9	8.6	3.2	2.6	3.6
16	3.8	4.0	2.4	6.1	16.3	3.5	4.3	9.4	6.8
17	1.6	1.9	4.1	4.7	3.8	10.2	5.6	3.6	7.7
18	1.5	3.5	5.2	2.1	1.4	2.7	4.3	2.3	2.7
19	1.3	2.0	7.2	4.0	2.2	2.3	9.3	2.5	4.6
20	1.2	1.7	2.8	6.1	4.9	3.6	3.8	2.1	8.8
21	1.1	2.2	5.8	2.1	1.7	5.4	4.1	2.4	2.6
22	1.1	1.6	4.2	3.0	1.1	2.6	3.6	1.9	2.3
23	1.0	1.8	2.7	9.7	4.2	4.3	3.5	1.6	3.3
24	6.9	1.2	1.3	3.1	1.9	6.4	3.5	1.3	14.9
Total	44.0	54.3	86.9	134.4	115.6	114.0	129.3	107.5	155.3
Mean	1.8	2.3	3.6	5.6	4.8	4.8	5.4	4.5	6.5
σ	1.4	0.7	2.1	3.8	3.4	2.7	2.4	2.7	5.2

Table F.2 Operator I - Tests 2, 3, and 4

	Test 2			Test 3			Test 4		
	J	M	P	K	N	Q	A	E	I
1	1.6	1.6	4.3	1.5	1.3	2.2	1.8	1.9	1.7
2	1.6	1.1	3.8	1.4	1.8	1.7	1.3	2.5	2.9
3	1.1	1.6	2.3	1.0	1.6	1.9	1.1	1.7	1.9
4	1.7	3.1	2.9	1.4	2.3	2.0	1.4	2.5	3.2
5	2.4	4.8	1.9	1.8	1.8	3.2	1.5	1.3	3.7
6	1.9	1.2	2.8	1.6	5.9	9.5	3.2	1.7	1.4
7	2.9	1.8	1.5	3.8	2.4	2.8	1.6	2.7	2.0
8	1.3	1.6	6.1	1.9	1.4	3.4	1.1	1.3	4.8
9	1.4	2.4	2.2	1.5	1.6	1.8	1.0	2.1	1.7
10	2.4	3.2	5.3	1.6	1.2	5.4	1.1	1.7	1.5
11	2.8	1.7	5.3	1.4	1.3	1.7	1.5	1.3	3.7
12	2.4	2.3	3.6	1.2	1.0	2.5	1.8	1.1	10.1
13	1.2	2.7	6.1	1.3	1.2	4.5	2.4	2.0	1.3
14	1.3	2.5	2.2	1.1	1.1	2.3	1.1	1.9	1.7
15	1.8	2.9	3.2	3.8	1.6	2.0	1.2	1.1	2.0
16	2.6	3.1	2.5	1.3	1.2	3.2	1.3	1.6	3.1
17	1.8	3.1	2.5	2.1	1.8	1.6	1.3	1.3	1.9
18	2.7	1.9	3.9	1.4	1.8	3.9	1.3	1.2	2.2
19	2.2	2.9	7.0	1.4	1.4	3.5	1.4	1.4	2.4
20	4.2	2.2	2.4	1.8	1.6	2.1	1.1	1.6	3.2
21	1.9	2.1	2.1	1.4	1.1	3.5	1.4	1.0	2.0
22	2.5	2.3	3.5	2.5	0.9	3.2	1.6	1.2	1.1
23	1.9	1.2	2.5	1.4	1.6	1.2	1.2	2.1	1.7
24	1.9	1.0	3.3	1.4	1.0	1.5	1.1	1.6	2.5
Total	49.8	54.3	83.3	41.1	40.1	70.7	35.1	40.0	63.7
Mean	2.1	2.3	3.5	1.7	1.7	2.9	1.5	1.7	2.7
σ	0.7	0.9	1.5	0.7	1.0	1.7	0.5	0.5	1.8

Table F.3 Operator I - Tests 5, 6, and 7

	Test 5			Test 6			Test 7		
	B	F	G	L	O	R	C	D	H
1	1.1	1.2	5.2	1.0	1.8	3.0	1.0	2.5	6.2
2	4.9	2.0	4.1	1.0	1.1	3.4	1.0	2.2	2.0
3	1.8	1.9	1.6	1.1	3.5	2.5	1.0	1.7	2.1
4	1.5	1.4	2.6	0.9	1.6	2.7	1.8	3.1	2.7
5	1.4	1.4	2.5	1.2	1.3	1.8	2.0	3.2	4.2
6	1.7	1.7	2.1	1.2	2.3	7.4	2.2	2.9	1.4
7	1.7	1.6	1.8	1.2	1.4	2.7	1.9	3.6	1.9
8	1.0	1.0	2.3	1.3	1.4	3.1	2.2	3.0	5.1
9	1.1	1.0	4.0	2.3	1.4	2.6	2.5	3.0	1.6
10	3.0	1.9	3.5	1.9	1.7	1.9	5.1	2.2	1.9
11	4.2	1.8	1.9	1.9	1.8	2.2	2.0	3.5	4.0
12	3.2	1.4	2.7	2.1	1.6	6.0	2.1	2.9	1.8
13	3.0	1.8	6.3	1.5	1.6	3.5	1.8	3.9	4.2
14	2.0	1.6	3.2	1.2	3.5	1.5	1.2	3.0	3.7
15	1.8	1.0	2.0	1.3	2.1	1.8	1.0	2.2	2.0
16	1.8	3.1	1.7	1.2	1.3	1.6	1.0	2.0	3.7
17	2.5	1.4	2.1	1.3	3.6	1.6	1.4	3.3	1.9
18	1.9	2.7	4.8	2.4	2.2	3.5	5.2	2.0	3.4
19	2.1	1.3	3.1	1.5	1.4	1.9	2.9	3.6	2.7
20	1.5	2.2	2.1	1.2	1.4	4.7	1.7	2.6	1.5
21	1.8	2.1	1.8	1.1	1.8	2.2	1.5	3.4	2.6
22	3.5	1.4	2.2	1.1	2.3	1.9	1.7	1.5	4.1
23	1.8	1.2	1.8	1.2	1.3	2.0	1.8	1.0	2.0
24	1.4	1.0	1.6	1.6	1.0	1.7	1.6	1.1	3.4
Total	51.9	39.5	67.1	33.7	44.7	67.1	47.8	63.6	70.2
Mean	2.2	1.6	2.8	1.4	1.9	2.8	2.0	2.7	2.9
σ	1.0	0.5	1.2	0.4	0.7	1.4	1.1	0.8	1.2

Table F.4 Operator II - Test 1

	60° FOV			30° FOV			15° FOV		
	J	M	P	K	N	Q	L	O	R
1	1.4	1.5	1.9	2.2	4.0	4.4	2.7	3.3	2.6
2	1.5	3.3	9.3	1.5	3.2	4.9	2.2	4.6	7.5
3	1.2	4.6	1.5	4.4	8.2	3.6	5.1	3.1	6.5
4	1.0	1.9	5.5	2.0	4.8	2.7	1.6	3.4	3.0
5	1.2	5.9	1.2	2.5	3.2	18.3	3.4	4.0	4.2
6	1.0	3.6	10.4	1.5	5.7	5.4	6.8	13.5	2.1
7	3.6	2.4	2.1	7.7	3.1	3.7	7.2	2.9	5.0
8	6.6	2.1	8.7	1.5	3.1	5.6	8.0	9.2	9.1
9	1.9	1.7	14.3	2.5	3.7	7.9	3.3	3.7	4.6
10	2.3	9.2	4.4	1.7	3.3	2.5	3.4	11.6	6.6
11	1.9	4.4	2.6	12.6	6.2	1.7	3.6	4.8	6.1
12	2.4	4.7	3.8	4.1	2.5	10.0	3.7	8.2	8.1
13	3.1	2.2	3.8	3.1	2.6	21.0	2.5	6.0	7.0
14	6.5	3.3	4.4	5.0	7.8	2.9	4.1	10.4	5.5
15	1.9	2.3	3.4	2.4	1.3	3.9	3.6	4.4	5.2
16	2.6	2.2	2.1	8.7	5.1	2.1	2.0	6.0	2.9
17	1.4	1.8	13.5	8.2	1.6	3.3	6.9	27.0	23.5
18	8.3	2.3	7.4	2.7	2.0	3.3	1.7	5.9	14.1
19	4.2	1.8	6.0	4.8	2.5	2.2	3.5	13.2	24.5
20	2.7	1.4	4.9	3.1	3.6	3.7	3.7	26.4	14.1
21	1.1	1.2	9.6	4.2	4.4	5.4	28.3	4.4	13.4
22	1.9	2.8	3.7	3.3	6.3	3.0	3.3	5.8	10.7
23	3.0	1.9	5.1	2.7	1.7	2.9	9.0	7.2	18.9
24	9.1	1.0	3.8	4.2	8.8	2.0	13.5	7.3	6.6
Total	72.1	69.7	133.3	96.9	99.0	126.6	133.4	196.4	211.6
Mean	3.0	2.9	5.6	4.0	4.1	5.3	5.6	8.2	8.8
σ	2.3	1.8	3.6	2.7	2.1	4.7	5.5	6.4	6.1

Table F.5 Operator II - Tests 2, 3, and 4

	Test 2			Test 3			Test 4		
	A	D	G	B	E	H	J	N	R
1	2.0	1.6	2.2	1.2	2.6	3.3	1.2	2.1	3.1
2	1.2	1.2	2.9	2.2	2.6	1.7	1.2	1.3	3.3
3	1.4	2.0	2.6	1.4	5.4	1.6	1.0	1.5	3.4
4	1.3	5.9	2.7	1.4	3.8	2.1	1.5	2.3	4.6
5	2.5	3.5	2.1	1.6	2.3	3.9	1.4	1.6	1.8
6	2.0	2.3	2.8	2.2	1.7	8.6	1.2	2.5	2.0
7	2.1	2.6	1.8	2.2	2.4	4.1	1.1	2.5	1.2
8	1.4	1.8	2.0	3.4	2.4	6.4	1.0	1.8	1.5
9	1.6	2.8	12.7	3.4	2.5	1.8	1.1	1.8	3.9
10	1.9	2.9	2.6	3.6	1.3	2.5	1.0	1.9	2.9
11	2.2	3.3	4.1	3.0	1.8	2.0	1.0	1.6	5.1
12	2.6	2.4	8.3	6.0	1.6	1.8	1.3	1.3	3.9
13	2.0	13.6	3.7	3.6	1.5	4.6	1.8	1.0	2.1
14	2.6	3.5	6.2	2.8	8.1	2.4	1.5	1.2	4.1
15	2.0	2.3	2.8	2.4	3.1	2.5	1.4	1.7	4.8
16	1.8	2.2	1.5	3.0	3.2	3.2	1.8	4.8	1.9
17	1.3	2.1	4.1	3.4	3.0	2.3	1.7	1.6	2.4
18	1.5	3.6	2.7	2.8	3.0	3.0	1.7	2.2	2.5
19	1.0	2.8	6.8	2.0	4.1	3.3	1.8	1.2	1.8
20	1.0	2.2	2.1	2.3	2.9	3.8	1.8	1.6	2.5
21	1.1	1.8	5.8	4.1	4.6	7.1	2.0	1.4	3.9
22	1.8	2.3	6.6	1.9	4.9	6.4	2.5	1.4	2.2
23	1.8	1.6	5.4	2.0	2.7	1.5	2.8	0.9	2.7
24	3.7	2.4	4.4	1.7	3.7	5.1	1.8	1.5	5.2
Total	43.9	72.6	98.9	63.8	75.3	85.0	36.8	42.7	72.9
Mean	1.8	3.0	4.1	2.7	3.1	3.5	1.5	1.8	3.0
σ	0.6	2.4	2.6	1.0	1.5	1.9	0.5	0.8	1.2

Table F.6 Operator II - Tests 5, 6, and 7

	Test 5			Test 6			Test 7		
	K	O	P	C	F	I	L	M	Q
1	1.1	2.3	5.2	1.3	1.2	3.2	2.0	2.5	2.1
2	1.0	2.1	3.9	2.7	1.5	5.3	1.7	2.0	2.8
3	1.2	2.7	2.8	3.0	2.3	2.8	1.7	2.5	3.8
4	1.3	2.5	2.6	2.1	1.1	3.7	5.4	2.2	2.8
5	1.1	2.3	2.5	1.8	2.8	2.9	2.9	2.2	4.5
6	1.2	2.4	1.4	2.8	2.2	2.4	2.0	6.0	4.0
7	1.0	2.1	1.5	1.7	1.4	1.8	2.3	2.7	2.9
8	1.1	2.5	2.1	1.7	1.3	2.1	4.6	2.9	2.3
9	1.7	1.5	2.2	2.6	1.9	2.3	3.4	2.4	2.9
10	2.0	1.3	3.0	2.4	1.9	2.0	4.0	2.0	2.4
11	2.0	1.4	2.7	2.0	1.8	5.2	2.0	2.2	4.0
12	2.3	4.4	1.8	2.0	2.3	9.5	3.3	2.5	1.5
13	2.5	2.5	2.7	1.6	1.2	5.1	2.2	2.7	3.1
14	2.2	1.9	3.5	2.3	1.9	5.1	1.4	2.5	3.0
15	2.4	1.5	2.2	2.7	1.7	1.4	2.6	2.9	4.9
16	2.4	2.0	2.3	1.6	1.3	2.5	5.3	3.1	5.1
17	1.9	2.5	1.8	1.6	2.8	2.8	2.5	3.3	9.5
18	1.6	3.0	3.0	1.6	2.2	4.1	2.5	3.6	2.8
19	2.0	3.4	2.2	1.4	1.2	2.4	2.4	2.2	2.3
20	1.5	1.9	2.1	1.6	1.9	3.0	2.4	2.1	2.4
21	2.1	1.4	5.5	1.8	2.1	5.3	2.7	1.8	3.5
22	5.1	1.1	4.6	1.7	1.1	10.4	1.7	2.1	4.3
23	2.4	1.2	1.9	2.0	1.6	3.8	2.0	2.7	4.3
24	1.9	1.2	3.1	2.1	3.9	5.5	4.1	1.2	1.7
Total	45.0	51.3	66.7	47.9	44.6	94.5	67.2	62.3	82.9
Mean	1.9	2.1	2.8	2.0	1.9	3.9	2.8	2.6	3.5
σ	0.8	0.8	1.1	0.5	0.6	2.2	1.1	0.9	1.6

Table F.7 Operator III - Test 1

	60° FOV			30° FOV			15° FOV		
	B	E	H	C	F	I	A	D	G
1	1.0	3.0	2.3	1.0	5.6	3.2	1.4	1.0	23.2
2	1.2	8.1	1.6	1.1	4.2	5.4	1.1	1.0	41.9
3	1.1	4.2	4.6	1.3	5.8	6.9	2.0	19.4	3.1
4	1.0	3.1	2.7	6.5	4.9	10.2	5.5	16.5	29.9
5	1.1	4.0	2.9	5.4	6.5	4.8	2.4	3.4	4.6
6	1.1	3.6	1.9	7.1	5.1	4.3	1.8	3.1	3.1
7	1.0	3.0	2.4	5.5	3.5	12.1	2.9	4.8	3.4
8	1.0	5.6	2.9	7.8	4.4	17.5	1.3	1.9	4.1
9	1.1	1.4	1.9	6.1	4.7	15.9	0.9	2.9	7.4
10	3.9	1.1	2.9	7.2	7.0	9.4	1.1	2.7	10.4
11	1.0	1.1	1.9	10.7	4.5	14.2	1.4	10.9	3.4
12	1.7	1.3	1.1	7.2	5.1	6.7	1.7	3.0	4.6
13	1.4	11.1	2.2	7.7	8.7	4.3	5.4	2.6	7.0
14	1.4	3.4	3.7	6.3	10.4	5.2	2.5	2.2	5.8
15	5.5	1.7	1.8	4.8	4.7	5.7	2.9	2.3	2.6
16	4.5	1.2	5.1	5.7	4.4	2.0	4.3	3.0	3.9
17	1.6	1.8	1.3	5.5	6.5	2.0	1.7	3.3	1.9
18	1.3	4.3	4.9	6.7	6.5	13.0	1.1	17.8	5.7
19	4.9	1.7	12.9	7.3	4.1	1.9	1.0	3.6	15.9
20	3.0	3.0	6.0	7.4	4.6	1.8	0.9	3.7	29.2
21	1.3	3.1	4.3	7.5	5.4	2.5	1.0	2.2	14.3
22	9.1	2.8	4.0	8.9	3.0	1.9	1.3	6.4	2.9
23	6.3	2.0	4.7	7.1	6.3	3.1	1.5	0.9	2.3
24	4.0	3.9	12.4	4.7	3.2	7.0	1.4	1.0	4.9
Total	60.6	79.6	92.4	146.5	128.9	160.9	48.5	119.6	235.4
Mean	2.5	3.3	3.9	6.1	5.4	6.7	2.0	5.0	9.8
σ	2.1	2.3	3.0	2.3	1.6	4.7	1.3	5.3	10.5

Table F.8 Operator III - Tests 2, 3, and 4

	Test 2			Test 3			Test 4		
	K	N	Q	L	O	R	B	F	G
1	1.4	2.9	2.9	1.0	1.7	1.3	1.9	1.6	6.6
2	3.1	1.9	1.8	1.0	1.9	2.2	3.7	1.2	3.7
3	3.4	3.7	2.6	3.3	2.3	1.2	2.7	1.8	8.8
4	3.4	1.9	3.6	2.8	3.5	2.5	1.2	4.2	2.6
5	2.0	1.9	2.6	10.5	1.4	1.5	2.1	4.0	2.6
6	2.9	2.2	2.4	4.5	4.4	1.2	5.8	2.6	3.1
7	2.0	1.8	7.5	1.2	1.7	1.5	1.2	1.3	1.9
8	2.0	3.2	4.7	1.8	2.0	2.2	2.2	1.7	2.0
9	1.4	2.9	1.8	2.2	7.9	1.5	1.7	2.4	4.4
10	2.1	1.5	8.2	2.4	6.4	2.0	2.8	1.0	6.3
11	3.9	1.7	3.9	2.1	2.2	3.8	2.2	1.3	4.7
12	3.1	2.3	1.6	1.6	1.2	2.2	2.2	1.4	2.5
13	6.9	1.4	7.4	5.9	3.4	1.8	2.5	1.3	3.8
14	2.7	2.0	3.1	1.0	1.7	4.1	1.4	1.6	2.7
15	1.6	2.3	2.8	1.0	1.6	2.4	1.5	1.2	2.3
16	5.3	3.2	3.1	1.1	4.4	2.7	2.1	1.6	3.0
17	2.5	2.6	2.0	1.2	2.4	2.9	1.7	2.5	1.9
18	2.0	2.1	2.9	3.4	6.8	1.2	1.6	2.3	4.2
19	1.9	2.6	2.0	1.6	3.1	2.3	2.7	1.6	3.7
20	2.1	2.4	2.8	10.4	1.2	5.7	2.3	1.3	2.1
21	2.3	1.5	3.9	2.2	3.0	3.3	2.5	1.7	2.1
22	2.9	1.1	3.1	1.7	2.0	2.2	1.9	1.7	2.5
23	2.6	1.8	6.3	1.0	1.1	1.8	2.6	1.1	1.4
24	2.2	1.2	2.2	1.0	1.9	5.9	2.2	1.3	5.1
Total	65.7	52.3	85.1	65.6	69.3	59.6	54.8	43.9	84.1
Mean	2.7	2.2	3.5	2.7	2.9	2.5	2.3	1.8	3.5
σ	1.2	0.6	1.9	2.6	1.8	1.3	0.9	0.8	1.7

Table F.9 Operator III - Tests 5, 6, and 7

	Test 5			Test 6			Test 7		
	C	D	H	J	M	P	A	E	I
1	1.0	2.1	1.7	1.1	2.6	1.1	1.6	2.5	2.1
2	1.0	1.0	1.0	0.9	1.5	3.6	1.9	2.4	6.9
3	1.0	2.1	2.2	4.3	2.3	2.1	2.1	5.5	6.3
4	1.3	6.3	2.3	1.6	4.0	2.4	2.0	2.5	4.0
5	2.2	1.5	2.1	1.2	7.2	1.5	1.2	3.5	4.7
6	4.7	1.5	2.1	1.1	2.5	4.8	2.1	2.9	2.2
7	1.7	2.2	1.6	1.0	1.9	2.0	2.4	6.3	4.4
8	4.5	1.7	3.3	1.0	1.7	4.2	1.5	4.6	3.9
9	4.2	2.3	1.7	1.1	1.4	2.9	2.4	2.6	2.7
10	5.8	1.2	3.9	1.0	6.0	4.1	2.6	1.9	2.7
11	2.0	2.4	3.1	1.4	2.6	4.2	2.1	2.0	7.6
12	5.0	2.3	1.8	1.0	3.8	3.9	2.8	3.1	6.9
13	2.4	2.4	2.5	0.9	3.4	4.7	5.7	1.9	4.7
14	2.0	2.4	1.5	1.2	3.3	6.2	2.3	1.8	1.6
15	1.7	2.6	1.9	1.0	2.9	3.9	1.9	1.7	1.8
16	1.5	2.0	2.2	1.9	2.6	2.7	3.1	2.0	3.6
17	1.4	1.9	2.7	1.6	2.2	3.0	3.6	1.3	3.4
18	1.5	2.4	2.4	1.1	3.4	2.7	1.1	3.2	7.3
19	2.5	2.2	2.6	5.7	3.6	3.4	2.4	2.1	3.9
20	1.1	4.1	2.3	1.5	3.8	3.8	2.6	3.8	2.1
21	1.2	1.1	4.6	1.4	2.6	4.3	1.7	10.6	4.1
22	1.1	1.0	5.1	1.6	2.4	7.1	2.6	3.6	1.9
23	2.6	1.0	2.2	0.9	1.9	2.6	5.2	2.9	2.2
24	2.5	1.0	1.9	1.7	1.7	1.6	2.5	2.9	2.8
Total	56.0	50.7	58.6	37.5	71.1	82.8	59.6	77.6	93.7
Mean	2.3	2.1	2.4	1.6	3.0	3.5	2.5	3.2	3.9
σ	1.4	1.1	0.9	1.1	1.3	1.4	1.0	1.9	1.8

Table F.10 Operator IV - Test 1

	60° FOV			30° FOV			15° FOV		
	K	N	Q	L	O	R	J	M	P
1	3.8	2.4	2.8	4.0	5.3	8.2	7.6	4.7	3.7
2	3.8	4.8	3.2	4.4	4.8	8.5	8.6	3.1	5.4
3	3.1	2.9	4.8	3.8	7.6	5.4	6.7	13.8	5.4
4	5.0	2.7	2.7	6.3	4.3	7.0	4.8	6.6	11.4
5	5.5	4.1	3.4	7.2	4.1	8.5	6.4	30.9	5.4
6	3.9	5.2	2.1	4.0	2.6	2.1	5.3	5.2	29.6
7	6.8	2.7	2.4	4.4	2.7	6.5	4.3	7.6	5.9
8	5.2	5.0	3.6	8.2	1.8	4.9	3.0	2.5	36.6
9	2.9	4.3	2.5	2.7	1.5	19.5	2.1	5.6	8.4
10	2.7	3.6	2.4	3.9	1.4	5.2	4.9	4.5	17.7
11	2.4	4.9	2.2	4.3	1.1	17.8	4.6	3.2	11.0
12	2.5	2.6	2.2	2.6	3.0	18.9	3.1	5.5	8.4
13	3.4	1.5	3.9	2.6	3.8	12.1	10.5	22.0	12.4
14	3.6	3.2	3.4	4.1	4.4	16.4	13.9	23.6	21.2
15	3.7	1.9	3.2	2.2	3.8	7.2	4.4	5.0	5.5
16	2.5	2.2	3.7	1.7	1.4	8.8	10.2	5.0	6.9
17	2.8	2.4	2.4	2.0	5.1	6.4	4.1	4.9	5.0
18	4.2	1.8	4.2	3.4	5.1	6.6	10.0	19.8	4.9
19	3.1	2.2	1.7	3.0	1.5	2.2	12.8	6.5	7.2
20	4.7	2.3	8.6	2.8	2.5	7.3	12.1	7.4	4.7
21	5.3	3.6	2.7	2.1	17.3	9.3	4.6	1.4	5.0
22	2.8	4.7	3.9	2.0	5.4	7.3	3.2	4.1	6.9
23	2.3	3.2	6.7	4.0	3.5	11.8	5.9	4.2	12.2
24	2.7	1.4	4.9	5.1	4.0	2.2	6.3	3.0	8.8
Total	88.8	75.6	83.4	90.6	98.0	210.3	159.7	200.1	249.6
Mean	3.7	3.2	3.5	3.8	4.1	8.8	6.7	8.3	10.4
σ	1.2	1.2	1.5	1.6	3.2	4.9	3.3	7.6	8.1

Table F.11 Operator IV - Tests 2, 3, and 4

	Test 2			Test 3			Test 4		
	B	E	H	C	F	I	K	O	P
1	1.1	1.7	2.1	1.1	1.6	2.2	1.2	1.1	3.0
2	2.0	2.3	1.3	1.2	4.0	2.6	2.3	1.8	4.3
3	1.6	2.3	3.7	1.0	2.3	1.9	1.8	2.6	2.0
4	1.7	2.9	2.9	1.2	1.8	6.1	3.6	2.8	2.4
5	1.7	3.7	4.9	1.8	1.3	3.1	2.1	2.3	1.6
6	1.4	2.2	2.2	1.5	1.7	2.4	1.6	1.9	1.6
7	1.3	1.8	2.9	1.3	1.9	1.8	1.7	1.3	1.9
8	2.3	2.3	2.1	2.3	1.9	1.4	1.1	3.0	2.5
9	2.1	2.0	2.0	1.9	1.8	2.3	1.2	1.8	2.7
10	3.8	2.2	1.7	5.9	1.6	2.1	1.4	1.0	3.2
11	3.9	2.6	1.7	2.0	1.8	7.6	1.6	4.3	1.3
12	2.0	1.4	6.3	1.8	3.2	5.4	1.8	1.6	8.4
13	1.4	1.0	2.3	1.4	1.6	5.5	1.4	1.4	3.3
14	1.4	1.6	2.5	1.1	2.2	6.3	1.2	1.8	1.8
15	1.2	1.2	2.9	1.3	3.6	1.8	1.5	1.8	2.2
16	1.3	1.7	4.0	1.4	2.7	2.2	1.8	1.3	5.6
17	5.0	1.2	3.1	1.2	1.8	1.8	1.8	1.8	4.0
18	1.5	2.0	3.7	1.4	1.2	2.5	1.5	1.4	4.7
19	4.1	1.9	6.7	1.3	1.4	1.2	1.7	1.1	4.1
20	2.1	1.9	2.1	1.6	1.1	2.0	1.6	1.3	2.3
21	2.0	2.0	4.0	1.1	1.1	2.4	4.7	1.4	1.8
22	4.3	1.7	3.1	1.3	1.8	1.9	1.9	1.4	4.1
23	1.4	1.1	2.2	1.1	1.5	1.5	3.4	1.0	1.1
24	1.0	1.1	1.8	1.0	1.0	1.8	2.6	1.0	3.1
Total	51.9	45.9	72.3	38.1	45.9	69.9	46.5	42.4	73.0
Mean	2.2	1.9	3.0	1.6	1.9	2.9	1.9	1.8	3.0
σ	1.1	0.6	1.4	1.0	0.8	1.8	0.8	0.8	1.6

Table F.12 Operator IV - Tests 5, 6, and 7

	Test 5			Test 6			Test 7		
	L	M	Q	A	D	G	J	N	R
1	1.1	1.7	1.9	1.9	1.5	2.6	1.2	3.3	1.2
2	1.2	1.1	1.1	2.9	1.7	2.4	1.4	3.5	3.9
3	1.0	1.8	1.9	2.0	1.4	2.1	2.3	3.0	7.5
4	1.4	1.4	1.7	1.3	6.5	2.9	1.7	2.6	2.8
5	1.3	1.1	1.9	1.2	3.1	1.6	1.3	2.3	1.8
6	1.2	1.1	1.7	1.3	1.2	1.6	1.3	2.4	4.4
7	1.9	1.4	6.1	1.6	1.4	1.9	1.4	2.6	2.7
8	1.3	1.1	1.7	1.3	1.4	2.8	1.4	2.6	3.0
9	1.2	1.3	1.6	2.2	2.1	2.7	1.5	1.4	3.0
10	1.8	1.5	4.1	2.0	2.5	4.8	1.2	2.0	2.0
11	1.4	1.9	1.5	1.0	1.9	2.2	2.1	1.6	4.2
12	1.4	1.8	1.6	1.1	2.0	3.4	2.6	2.0	4.3
13	3.9	1.4	1.9	1.0	2.7	4.0	2.8	1.2	3.8
14	1.1	2.4	2.1	1.2	2.4	8.1	2.6	2.0	10.0
15	1.0	2.0	11.4	1.1	1.4	3.1	2.0	1.4	2.6
16	1.0	1.6	2.1	1.0	6.2	2.2	3.7	2.4	2.7
17	5.2	1.5	3.9	1.1	2.6	4.8	2.5	1.7	2.1
18	1.4	3.0	5.1	0.9	2.4	4.0	1.3	1.8	2.4
19	1.3	1.6	2.3	1.1	2.9	5.0	1.3	2.0	1.2
20	1.3	1.7	3.1	2.0	2.2	1.7	2.5	1.8	2.8
21	1.5	0.9	3.3	1.7	2.1	1.8	3.2	2.3	3.1
22	1.3	1.0	2.5	1.3	1.7	2.4	1.8	1.3	2.1
23	1.1	1.0	1.4	1.0	1.2	1.5	1.5	2.0	2.8
24	1.0	1.0	2.4	5.0	1.1	3.1	2.7	1.4	1.9
Total	37.5	36.5	68.3	38.5	55.7	72.9	47.4	50.7	78.2
Mean	1.6	1.5	2.8	1.6	2.3	3.0	2.0	2.1	3.3
σ	1.0	0.5	2.2	0.9	1.3	1.5	0.7	0.6	1.9

APPENDIX G

Operator Learning Curves

Estimation of the operators' learning curves involved four assumptions.

- The learning curves had positive slope at all times.
- The learning curves were smooth functions.
- The learning curves were exponential functions.
- For a specified field of view, operator learning was reflected primarily in the standard deviation of the normalized course times (a smoothness measure).

Each operator drove 21 courses with a 60° field of view, three for each of the seven tests. The procedure below was applied to the normalized data for each operator to estimate his 60° FOV learning curve.

- The standard deviations were entered into a 3 x 7 matrix. Each row represented a specific window width β as discussed in section 5.2 (row 1 = 15°, row 2 = 30°, and row 3 = 60°). Each column corresponded to a given test (column 1 = test 1, column 2 = test 2, etc.).
- The standard deviations for the three window widths for each test were summed and entered into a row vector of seven elements. Each column continued to represent a given test as above. This step yielded the summed standard deviations (SSD).
- The row vector elements were plotted with summed standard deviations on the vertical axis versus test number on the horizontal axis.
- An exponential curve using the method of least squares was fitted to the plot by linearizing the exponential form through taking logarithms [G-1]. This

defined the operator's 60° FOV learning curve.

Figures G.1 through G.4 show the learning curves (graphed as lines) versus the test number.

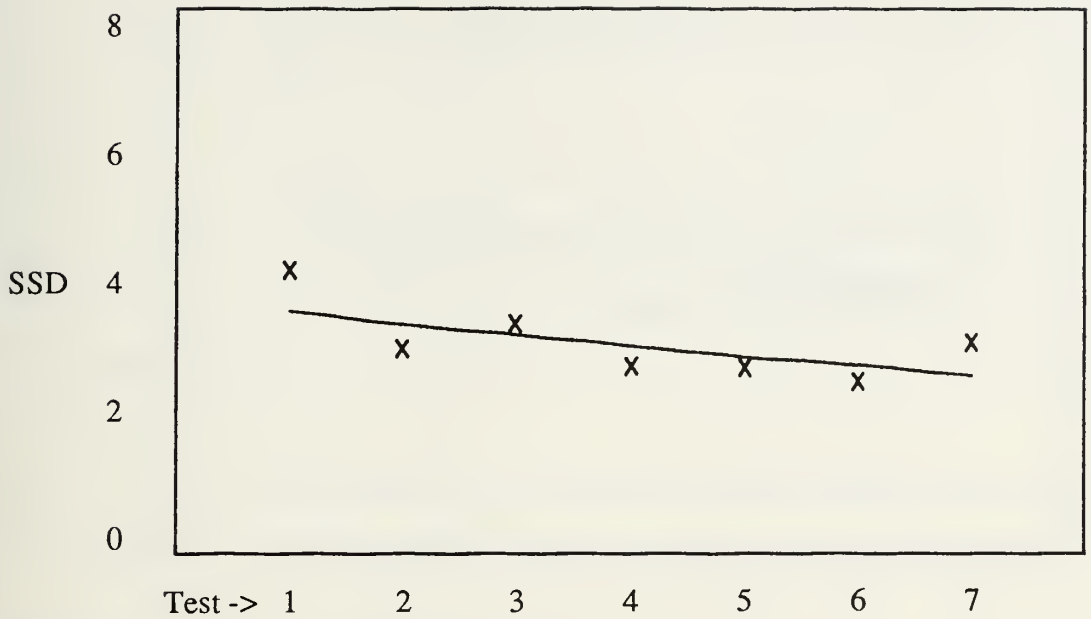

Figure G.1 Operator I 60° FOV learning curve

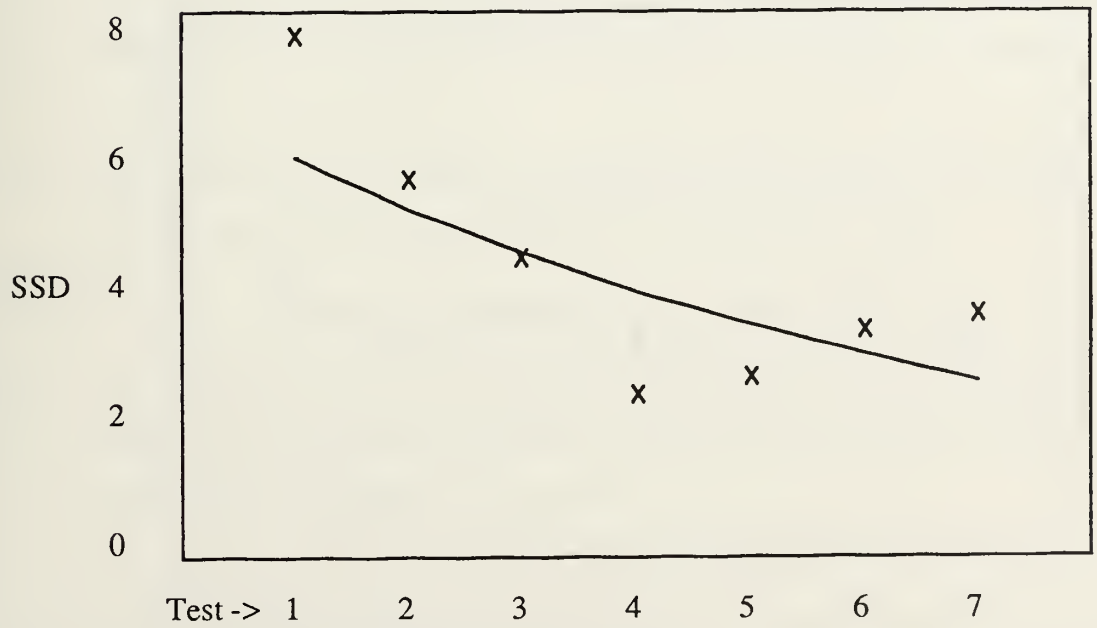

Figure G.2 Operator II 60° FOV learning curve

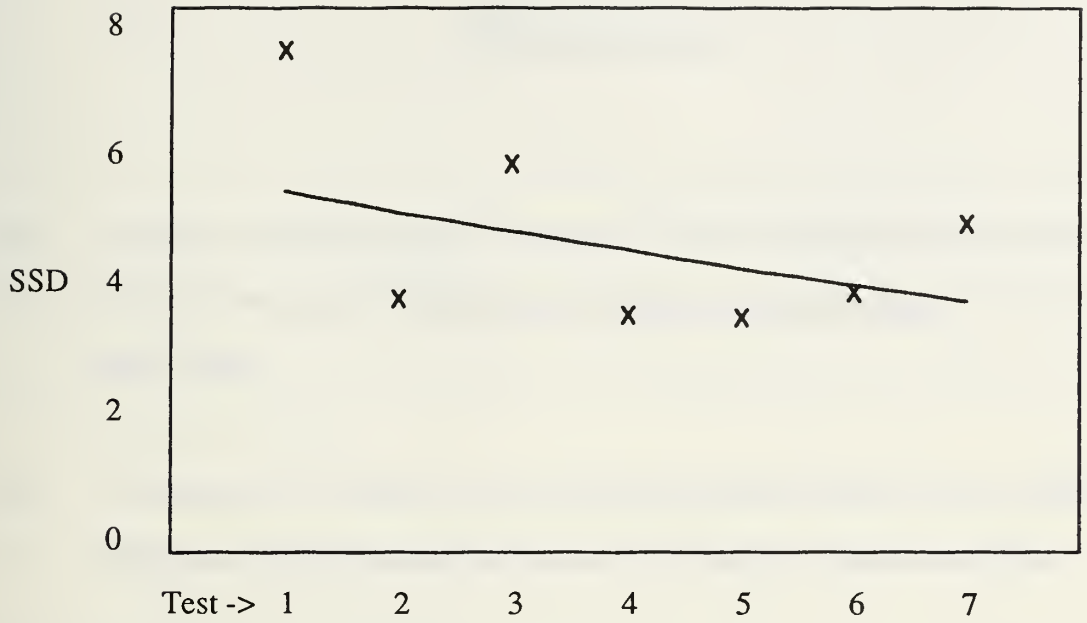

Figure G.3 Operator III 60° FOV learning curve

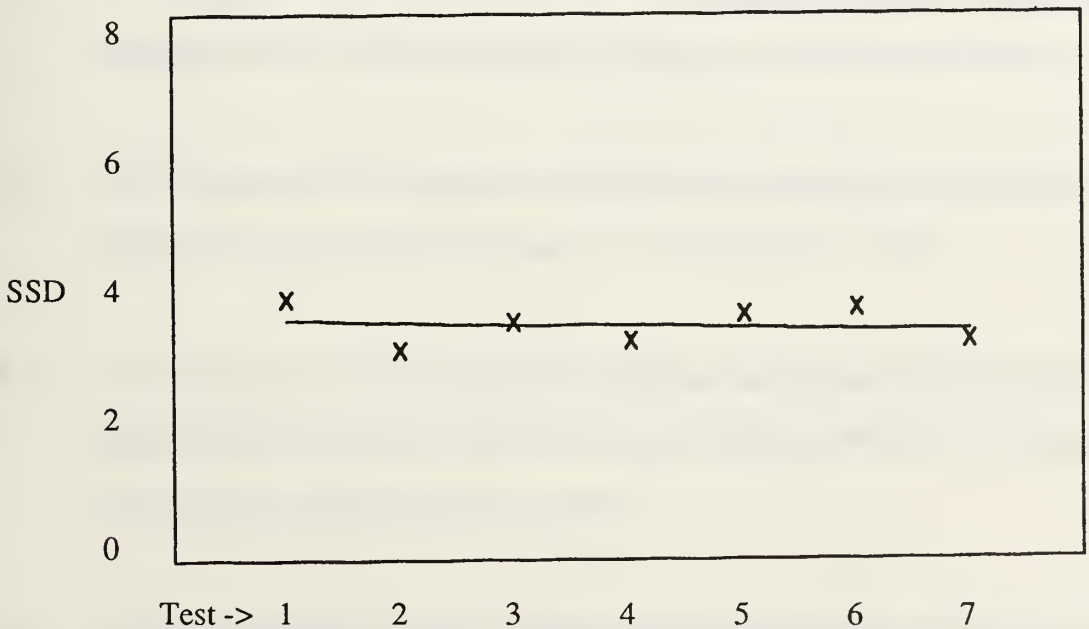

Figure G.4 Operator IV 60° FOV learning curve

APPENDIX H

References

B-1 T. Berk, L. Brownston, and A. Kaufman, "A New Color-Naming System for Graphics Languages," IEEE Computer Graphics and Applications, Vol. 2, No. 3, (May 1982).

C-1 I. Carlbom and J. Paciorek, "Planar Geometric Projections and Viewing Transformations," ACM Computing Surveys, Vol. 10, No. 4, (December 1978).

E-1 A. Emmett, "In Search of the Miracle Hologram," Computer Graphics World, Vol. 14, No. 2, (February 1991).

F-1 J. D. Foley, A. van Dam, S. K. Feiner, et al., Computer Graphics: Principles and Practice, Addison-Wesley Publishing Company, Inc., Reading, MA, 1990.

G-1 C. F. Gerald and P. O. Wheatley, Applied Numerical Analysis, fourth edition, Addison-Wesley Publishing Company, Inc., Reading, MA, 1990.

K-1 K. L. Kelly and D. B. Judd, COLOR: Universal Language and Dictionary of Names, National Bureau of Standards Special Publication 440, U. S. Government Printing Office, Washington, D. C., 1976.

M-1 D. Meister, Behavioral Analysis and Measurement Methods, John Wiley & Sons, Inc., New York, 1985.

M-2 F. H. Moffitt and E. M. Mikhail, Photogrammetry, third edition, Harper & Row, Publishers, Inc., New York, 1980.

S-1 M. S. Sanders and E. J. McCormick, Human Factors in Engineering and Design, sixth edition, McGraw-Hill Book Company, New York, 1987.

S-2 L. D. Sher, personal communication, BBN Laboratories Incorporated, interview February 12, 1991.

S-3 I. E. Sutherland, "The Ultimate Display," in Proceedings of the 1965 IFIP Congress, 2, 1965, 506-508.

S-4 I. E. Sutherland, "A Head-Mounted Three Dimensional Display," in FJCC 1968, Thompson Books, Washington, DC, 757-764.

S-5 W. K. Stewart, "A Non-Deterministic Approach to 3-D Modeling Underwater," in Proceedings of the Symposium on Unmanned Untethered Submersible Technology, Vol. 1, University of New Hampshire, Marine Systems Laboratory, (June 1987).

S-6 W. K. Stewart, "Multisensor Modeling Underwater with Uncertain Information," Ph.D. Thesis, Massachusetts Institute of Technology and Woods Hole Oceanographic Institution, (September 1988).

S-7 W. K. Stewart, ""Visualization Resources and Strategies for Remote Subsea Exploration," Scientific Visualization of Physical Phenomena, Springer-Verlag,

Hong Kong, 1991, 85-109.

T-1 A. C. Traub, "Stereoscopic Display Using Rapid Varifocal Mirror Oscillations," Applied Optics, Vol. 6, No. 6, (June 1967).

Biographical Note

Lieutenant Commander Larry Galvin graduated with distinction from the United States Naval Academy in 1978 with a Bachelor of Science degree in Mathematics. His eleven years of service in the Submarine Force has included tours on USS Skate (SSN-578), USS Whale (SSN-638), and USS Jack (SSN-605). Following completion of graduate work, LCDR Galvin will report to USS Buffalo (SSN-715) as Executive Officer.